

Modified N-linked glycosylation status predicts trafficking defective human Piezo1 channel mutations

Jinyuan Vero Li¹, Chai-Ann Ng^{1,2}, Delfine Cheng^{1,2}, Zijing Zhou¹, Mingxi Yao³, Yang Guo^{1,2}, Ze-Yan Yu^{1,2}, Yogambha Ramaswamy⁴, Lining Arnold Ju⁴, Philip W. Kuchel⁵, Michael P. Feneley^{1,2,6}, Diane Fatkin^{1,2} & Charles D. Cox^{1,2}  

Mechanosensitive channels are integral membrane proteins that sense mechanical stimuli. Like most plasma membrane ion channel proteins they must pass through biosynthetic quality control in the endoplasmic reticulum that results in them reaching their destination at the plasma membrane. Here we show that N-linked glycosylation of two highly conserved asparagine residues in the ‘cap’ region of mechanosensitive Piezo1 channels are necessary for the mature protein to reach the plasma membrane. Both mutation of these asparagines (N2294Q/N2331Q) and treatment with an enzyme that hydrolyses N-linked oligosaccharides (PNGaseF) eliminates the fully glycosylated mature Piezo1 protein. The N-glycans in the cap are a pre-requisite for N-glycosylation in the ‘propeller’ regions, which are present in loops that are essential for mechanotransduction. Importantly, trafficking-defective Piezo1 variants linked to generalized lymphatic dysplasia and bicuspid aortic valve display reduced fully N-glycosylated Piezo1 protein. Thus the N-linked glycosylation status *in vitro* correlates with efficient membrane trafficking and will aid in determining the functional impact of Piezo1 variants of unknown significance.

¹Molecular Cardiology and Biophysics Division, Victor Chang Cardiac Research Institute, Sydney, Australia. ²St Vincent’s Clinical School, Faculty of Medicine, University of New South Wales, Sydney, Australia. ³Mechanobiology Institute, National University of Singapore, Singapore, Singapore. ⁴School of Biomedical Engineering, Faculty of Engineering, The University of Sydney, Camperdown, NSW, Australia. ⁵School of Life and Environmental Sciences, University of Sydney, Sydney, NSW, Australia. ⁶Department of Cardiology, St Vincent’s Hospital, Sydney, Australia. ✉email: c.cox@victorchang.edu.au

The Piezo family of ion channels has only two members, Piezo1 and Piezo2^{1,2}. These are large membrane proteins with more than 30 transmembrane helices that decode mechanical cues. Piezo1 in particular appears to be a central mechanotransducer in the cardiovascular system^{3,4} and is sensitive to membrane forces^{2,5–7} and thus lipid composition^{8–12}. Like many other integral membrane proteins, Piezo1 channels undergo biosynthetic quality control during their biogenesis¹³. This study focussed on exactly how these processes regulate the membrane expression of Piezo1.

Almost all membrane proteins undergo folding and maturation in the ER, where N-linked glycosylation usually fulfils a critical role in biosynthetic quality control^{13,14}. N-linked glycosylation is the process by which oligosaccharides are covalently attached to asparagine residues in proteins, at specific asparagine containing motifs. This process begins with the co-translational addition of core-glycans in the ER and culminates in the processing, modification and potential elongation of the N-glycan in the Golgi prior to vesicular transit to the plasma membrane. The larger N-glycans that result from the extension of the core-glycan unit can be: (1) high mannose, (2) complex, or (3) hybrid glycans, depending on the number and types of carbohydrates that are added^{13,15}. Once the N-glycans are added to the membrane protein, they aid in the folding process and usually enhance protein stability^{16,17}. In many cases, the N-glycans act as a ‘quality control stamp’ certifying the membrane protein is folded correctly during its biosynthesis.

It is particularly evident that N-linked glycosylation is important in the biosynthetic quality control of plasma membrane ion channels. The hERG K⁺ channel (K_{v11.1})^{18,19}, cystic fibrosis transmembrane conductance regulator (CFTR)²⁰ and polycystic kidney disease proteins²¹ have all been studied in this regard. Variants in these ion channels cause channelopathies that arise from two broad mechanisms: (1) a functional defect in the channel; or (2) aberrant plasma membrane trafficking. In fact, most disease-causing variants are aberrantly trafficked. For example, in the case of K_{v11.1} mutations, ~80% of variants linked to long QT syndrome type II (LQTS2) ameliorate trafficking²². The N-linked glycosylation of K_{v11.1} produces a characteristic pattern on a western blot consisting of a fully glycosylated protein of larger molecular size (~155 kDa), and a core glycosylated protein that is smaller (~135 kDa)^{18,19,22–25}. The upper band (larger molecular size) is a surrogate for the mature membrane protein¹⁷ and as a result, has been used extensively to interrogate disease linked variants of unknown significance in K_{v11.1}^{22,24,26}. Specifically trafficking-defective channel mutants lack the mature form of the protein, and rather than showing a double band appearance on a western blot they have a single band that represents the core-glycosylated protein. Given that variants of *PIEZO1* have been linked to disease (e.g., generalised lymphatic dysplasia^{27,28} and bicuspid aortic valve²⁹), we explored whether human Piezo1 undergoes N-linked glycosylation and whether this serves as a predictor of efficient membrane trafficking.

Here, we report on the molecular events that occur during the trafficking of Piezo1 channels, and we showed that N-linked glycosylation was critical in the biosynthetic quality control of this channel. In particular, we demonstrated a novel mechanism whereby two highly conserved asparagines in the cap (N2294Q and N2331Q), which are essential for normal trafficking of Piezo1 to the plasma membrane, dictated the glycosylation status of the propeller domains that extend out from the central ion conducting pore^{30–32}. Also, the presence of the larger N-glycosylated species of Piezo1 was seen to be a surrogate for the mature membrane protein as it was absent in trafficking-defective mutants. These findings will be useful when assessing the effects of mutations generated during structure-function

studies³³, or when exploring disease-linked *PIEZO1* variants. As a proof of concept, we showed that loss-of-function Piezo1 variants such as G2029R that are known to be trafficking-defective²⁸ lack a larger N-glycosylated species when expressed in vitro. Furthermore, we revealed that some loss-of-function variants that affect trafficking display a dominant negative effect on function, and retard the trafficking of the wild-type protein. These findings have broad significance for future studies of diseases resulting from *PIEZO1* variants.

Results

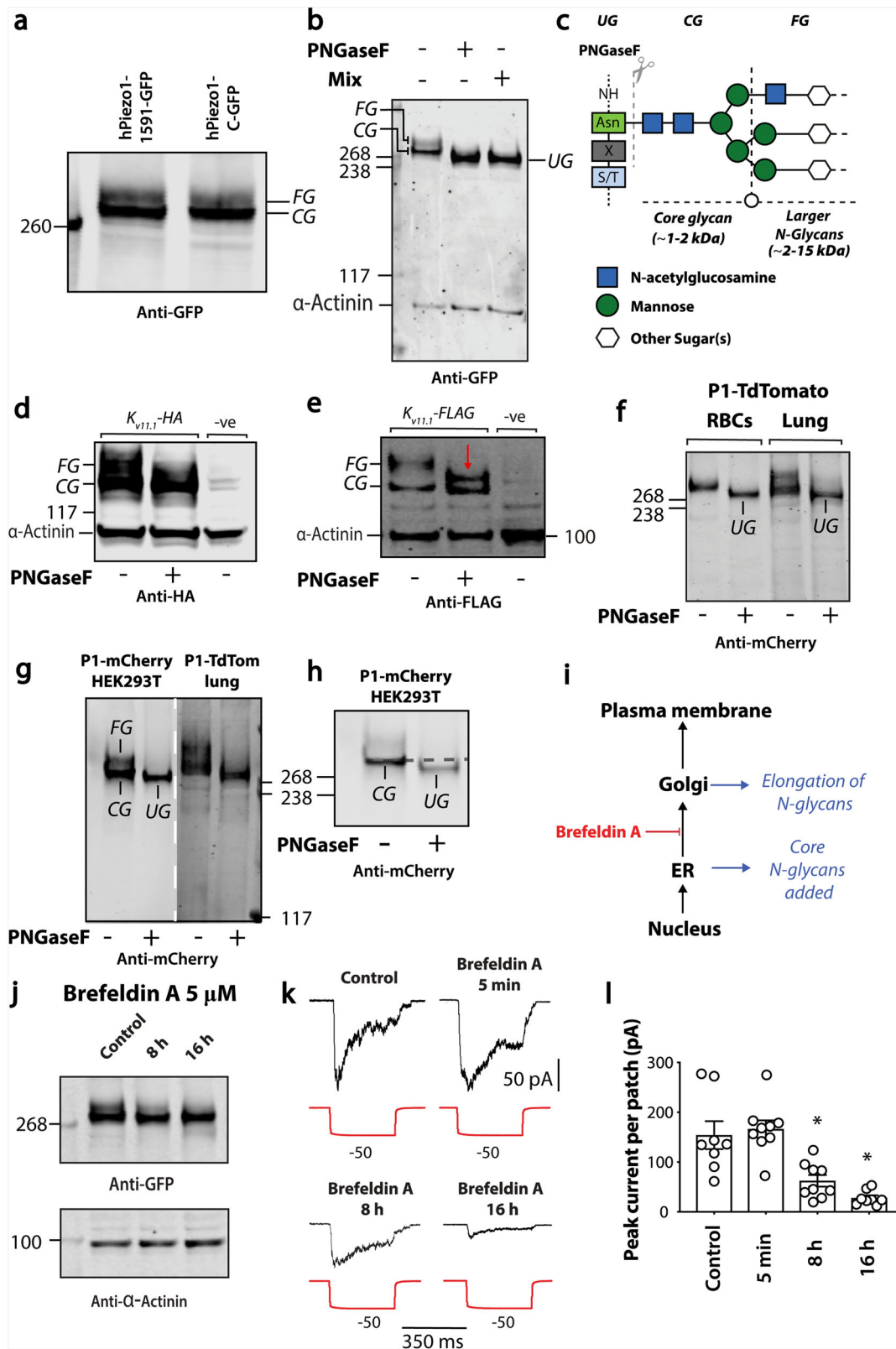
N-linked glycosylation of heterologously expressed Piezo1

First, we used Piezo1 fusion proteins to probe Piezo1 expression because there are no specific anti-Piezo1 antibodies; instead we exploited highly specific antibodies to GFP and mCherry. This allowed us to correct for minor variability in transient transfection by using the GFP or mCherry fluorescence intensity of the cell lysate, to calculate the relative amounts required to load for western blotting. Initial trials at probing Piezo1 expression in Piezo1^{-/-} HEK293T cells with western blotting showed extensive smearing in the lanes³⁴. This was corrected by adding a reducing agent during cell lysis, thus preventing protein cross-linking and aggregation. Supplementary Fig. 1a shows gels run using samples without reducing agents in RIPA buffer compared with samples with 5 mM β-mercaptoethanol, 5 mM TCEP or 10 mM of the alkylating agent NEM, during cell lysis. We found that NEM treated Piezo1 was slightly larger in molecular size due to the large number of cysteines present in Piezo1. Specifically, if all 57 -SH groups were in a reduced state before modification with NEM (0.125 Da) there would have been an increase in size of 57 × 0.125 Da = 7.125 kDa, thus resulting in a significant net increase.

Piezo1 expressed in HEK293 cells resembled Piezo1 from native mouse tissue (specifically aorta)³⁵, which on western blots showed two distinct bands (Fig. 1a, b and Supplementary Fig. 2; fully glycosylated—FG; core glycosylated—CG and UG—unglycosylated). The molecular basis of these two bands has not been investigated. To determine if the two bands resulted from different extents of glycosylation, Piezo1-GFP lysates were incubated with PNGaseF that only hydrolyses N-linked glycans, and a mixture of deglycosylases that hydrolyse N-linked and O-linked oligosaccharides. Figure 1b shows the upper band (labelled fully glycosylated—FG) was absent after treatment, while the lower band had increased mobility suggesting reduced size. The molecular correlates of the UG, CG and FG bands are illustrated pictorially in Fig. 1c. PNGaseF alone and the mixture of deglycosylases produced the same effect. The estimated size difference on the removal of N-linked oligosaccharides, based on the calibrating ladder on the gel, was 20–30 kDa.

As a positive control for PNGaseF digestion we used K_{v11.1} the hERG potassium channel. This channel is known to undergo N-linked glycosylation and migrates as two species (Fig. 1d, e), a core glycosylated protein (CG, ~135 kDa) and a fully glycosylated protein (FG) of higher molecular size (~155 kDa)¹⁸. On treatment with PNGaseF, we also saw cleavage of the upper band regardless of which tagged version of the protein was used. This included the generation of a previously reported PNGaseF resistant modification shown in Fig. 1e, labelled with a red arrow.

N-glycosylation of endogenous Piezo1. The next experiments addressed the question of N-linked glycosylation in cell types that natively express Piezo1. Here, we studied red blood cells (RBCs) and lung tissue that are known to have high levels of expression of Piezo1¹, isolated from a Piezo1-TdTomato reporter mouse. Figure 1f shows that in both RBCs and lysate from lung tissue



that the molecular size that Piezo1 runs at is reduced by treatment with PNGaseF. Furthermore, the extent of glycosylation was not altered by the TdTomato tag.

We compared human Piezo1-1591-mCherry to mouse Piezo1-TdTomato extracted from lung tissue that had different tags fused at different positions (Fig. 1f, g). While the sample of mPiezo1-TdTomato fusion protein was larger (~320 kDa), it still clearly

contained the species of larger molecular size (N-glycosylated version), which was reduced in size in the sample that had been treated with PNGaseF. In comparison to the extracts from HEK293 cells and lung tissue, only one band was observed in the RBC lysate it became smaller on PNGaseF treatment (Fig. 1f).

To explore further where in the cell the larger N-glycans (that we now refer to as ‘full’ glycosylation) were added to Piezo1, the

Fig. 1 N-linked and glycosylation of Piezo1 in a heterologous expression system and in native cell types. **a** A representative western blot of hPiezo1-1591-GFP and Piezo1-C-GFP expressed in HEK293 cells. **b** A representative western blot illustrating cleavage of the upper FG (fully glycosylated) band of the Piezo1 doublet in the presence of the enzyme PNGaseF and a mix of O-linked and N-linked deglycosylase (CG—core-glycosylated, UG—unglycosylated). **c** Schematic illustration of PNGaseF mediated cleavage of N-linked glycans at the molecular level. **d** Representative western blot showing the effect of PNGaseF digestion on $K_{v11.1}$ -HA and **e** $K_{v11.1}$ -FLAG protein expressed in HEK293 cells. The red arrow denotes a previously identified PNGaseF resistant $K_{v11.1}$ component. **f** Representative western blot comparing the effect of PNGaseF digestion of mouse Piezo1-TdTomato from red blood cells (RBCs) and lung tissue. **g** Comparison of western blot of human Piezo1-1591-mCherry expressed in HEK293 cells with mouse Piezo1-TdTomato from mouse lung tissue (different exposure denoted by dashed white line). **h** Reduced intensity, of representative blot shown in **g** to illustrate the reduction in size of the lower CG band in addition to the loss of the upper FG band. **i** Schematic representation of where N-glycans are added and the site of action of the fungal metabolite brefeldin A. **j** Representative western blot of brefeldin A treatment (0–16 h) on human Piezo1-GFP expressed in HEK293 cells. **k** Raw electrophysiological traces from cell-attached patches of brefeldin A treated Piezo1^{-/-} HEK293T expressing Piezo1-GFP recorded at -65 mV. **l** Quantification of peak Piezo1 currents per patch elicited by negative pressure pulses in the presence of brefeldin A for escalating durations. Data expressed as mean \pm SEM * $p < 0.05$ determined by Kruskal-Wallis test with Dunn's post-hoc test.

trafficking between the ER and Golgi was inhibited with brefeldin A (Fig. 1i). This fungal metabolite prevents movement of proteins from the ER to the Golgi by disassembling transport vesicles³⁶. Treatment of cells with brefeldin A led to the accumulation of the lower band on western blots, and after 12–16 h the upper fully glycosylated version was no longer evident (Fig. 1j). Therefore, we concluded that the larger N-glycans were added to Piezo1 in the Golgi.

If, like $K_{v11.1}$, the fully glycosylated form of Piezo1 was indicative of the mature membrane protein, then brefeldin A treated (>12–16 h) cells should have reduced stretch-activated currents. Indeed, the peak stretch-activated currents recorded from Piezo1^{-/-} HEK293T cells heterologously expressing Piezo1-GFP, compared to those from untreated or acutely treated cells were reduced (Fig. 1k, l). The average current per patch for Piezo1-GFP expressed in Piezo1^{-/-} HEK293T was 154 ± 28 pA ($n = 8$), and this was reduced ~6-fold to 27 ± 5 pA ($n = 8$) after 16 h treatment with brefeldin A. This brefeldin A effect was not due to ion channel blockade of Piezo1 as a 5 min acute treatment with brefeldin A did not affect Piezo1 currents, 164 ± 22 pA ($n = 7$) (Fig. 1k, l).

While probing tagged versions of Piezo1 we identified the same double band in the untagged Piezo1, using a newer mouse monoclonal anti-Piezo1 antibody (Cat. No. NBP2-75617, Novus Biologicals). This antibody reproducibly recognised human Piezo1, which presented as two bands on a western blot. Importantly, untransfected Piezo1^{-/-} HEK293T cells served as a negative control (Supplementary Fig. 1b). This antibody also recognised native Piezo1 in human RBCs, but failed to recognise mouse Piezo1-GFP recombinantly expressed in Piezo1^{-/-} HEK293T cells. This finding was confirmed when the same western blot was probed with a GFP antibody (Supplementary Fig. 1b). Hence, we concluded that the untagged protein also underwent glycosylation, and that a tag does not influence N-glycosylation.

Endogenous Piezo1 in immortalised human fibroblasts also showed two bands on a western blot (Fig. 2a). The higher molecular weight band was much more intense than that of human Piezo1 that had been transiently expressed in HEK293 or Neuro2A cells (Fig. 2a, b and Supplementary Fig. 3). The ratio of the upper band compared to the lower band was >10-fold higher in fibroblasts (Fig. 2b). The upper band was assigned to the N-glycosylated protein since treatment with PNGaseF decreased the molecular size, giving coalescence of both bands (Fig. 2a).

We sought to determine whether the upper band, assigned as the N-glycosylated protein, represented the fully mature plasma membrane protein. For this we used a method to 'unroof' fibroblasts. This protocol removes apical plasma membranes, nucleus, and organelles and leaves only the basal membrane attached to the tissue culture substrate (Fig. 2c). The procedure has been widely used in conjunction with various imaging

methods^{37,38} and also proteomics³⁹, but it has rarely been used for studying plasma membrane localisation.

Proof of successful unroofing was obtained by staining for the focal adhesion protein vinculin, and imaging with epifluorescence microscopy (Fig. 2d). While focal adhesions containing vinculin were not clearly defined with intact cells, focal adhesions labelled with vinculin became well defined once the cells were unroofed. We and others have shown that Piezo1 is present in the basal membrane of fibroblasts^{40,41}, so western blots were performed on extracts from intact and unroofed cells. From unroofed cells, only the upper band, which was assigned to the glycosylated protein remained (Fig. 2e and Supplementary Fig. 4), and the unroofed cells also lacked α -tubulin as previously reported³⁹. We concluded that the mature membrane pool of Piezo1 in fibroblasts was highly N-glycosylated. This was supported by experiments illustrating only the FG version was biotinylated (Fig. 2f). Furthermore, these experiments confirmed that endogenous Piezo1 in human fibroblasts underwent N-linked glycosylation in a manner similar to Piezo1 that was transiently expressed in HEK cells, Neuro2a cells, and endogenous Piezo1 in mouse lung tissue. Finally, unlike heterologous systems where large amounts of protein are produced, the fully N-glycosylated Piezo1 was the larger proportion of natively expressed Piezo1 in fibroblasts.

Piezo1 N-glycosylation of two Asn residues in the cap. Having established the existence of N-glycosylation of Piezo1, we sought specification of the sites of this post-translational modification. The on-line programme NetNglyc1.0⁴² predicted nine sites that could be N-linked, six in the N-terminus and three in the C-terminus. The three asparagines identified by NetNglyc1.0 in the C-terminal domain are in the cap or C-terminal extracellular domain (CED)^{31,32}, one of which is buried and seems unlikely to accept N-glycosylation, while the other two are freely accessible from the extracellular space (Fig. 3a). Previous mass spectrometry identified a glycosylated peptide corresponding to one of these predicted asparagines (N2331)⁴³. Both asparagines are highly conserved in homologues of Piezo1 and have the classical signature sequence Asn-Xaa-Ser/Thr for N-linked glycosylation (Fig. 3b). In contrast, these Asn residues are not conserved in Piezo2; but a recent Cryo-Electron Microscopy (Cryo-EM) structure of mouse Piezo2 shows at least one glycan in the cap region⁴⁴. Therefore, to test if the fully glycosylated Piezo1 protein was dependent on either of these asparagines, we created single mutants (N2294Q, N2331Q), and a double mutant (N2294Q and N2331Q; also called 'CapQQ').

Only a minor decrease occurred in the amount (as measured by western blots) of the fully glycosylated species in the single mutants, but there was complete abolition of the upper band in the double mutant (N2294Q and N2331Q) (Fig. 3c), which mirrored the effect of treatment with PNGaseF.

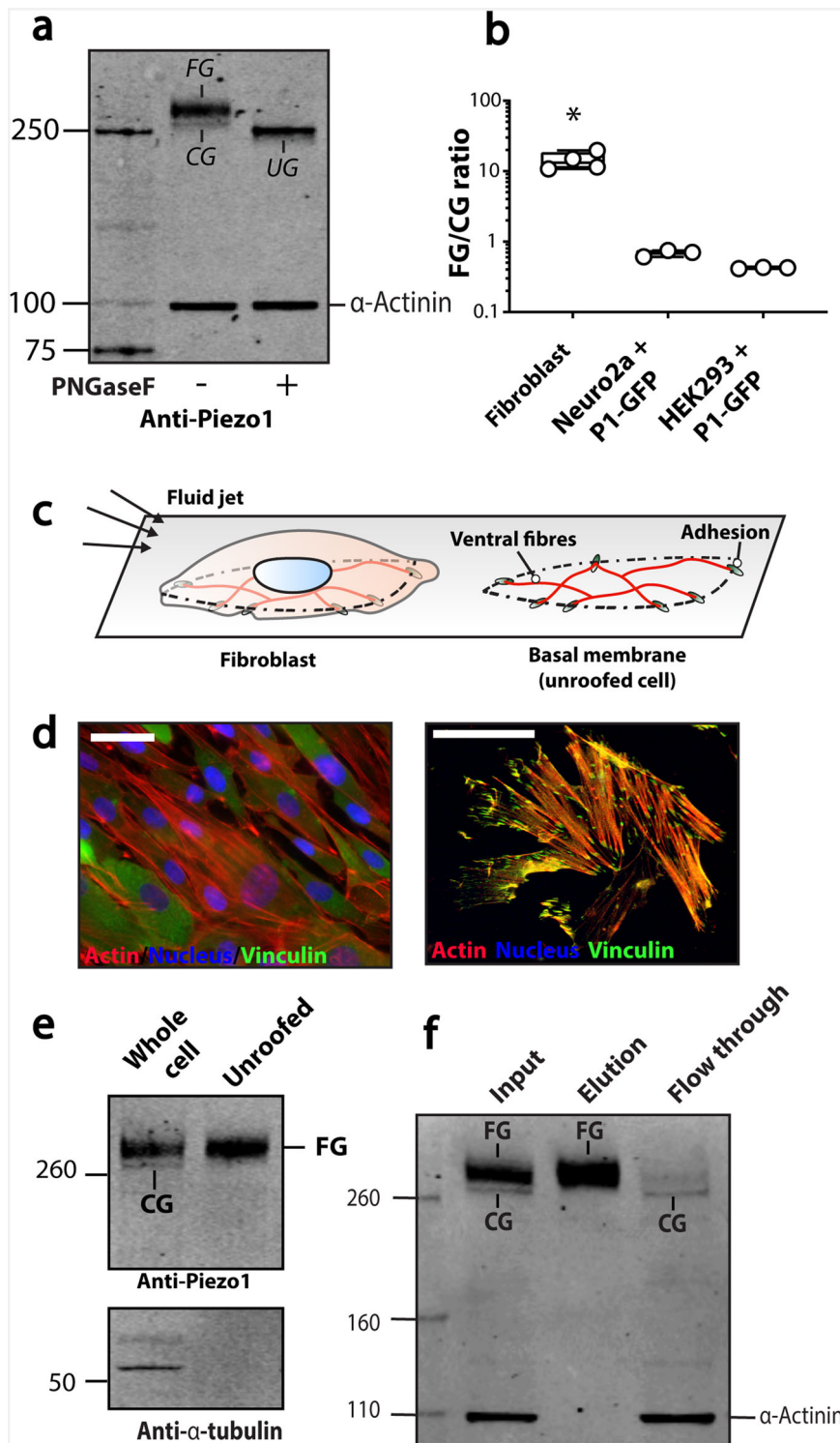


Fig. 2 N-glycosylation of endogenous Piezo1 in human fibroblasts. **a** A representative western blot of untreated immortalised human foreskin fibroblasts versus PNGaseF treated fibroblast lysate probed using the anti-Piezo1 antibody and anti-α-actinin antibody as a loading control. **b** The ratio [FG/CG] of the upper band (FG) and lower band (CG) of fibroblast Piezo1 and Piezo1 heterologously expressed in Neuro2A and HEK293T. **c** Schematic illustration of an intact fibroblast, and an unroofed fibroblast. **d** A representative image of an intact fibroblast (left panel), and an unroofed fibroblast (right panel) using standard wide-field microscopy and a 63× oil objective. **e** A representative western blot of intact fibroblast lysate versus unroofed fibroblast lysate probed using anti-Piezo1 antibody and anti-α-tubulin antibody as a loading control to confirm unroofing. **f** A representative western blot of biotinylated immortalised human foreskin fibroblasts. (CG core-glycosylated, FG fully glycosylated) **p* < 0.05 determined by Kruskal-Wallis test with Dunn's post-hoc test.

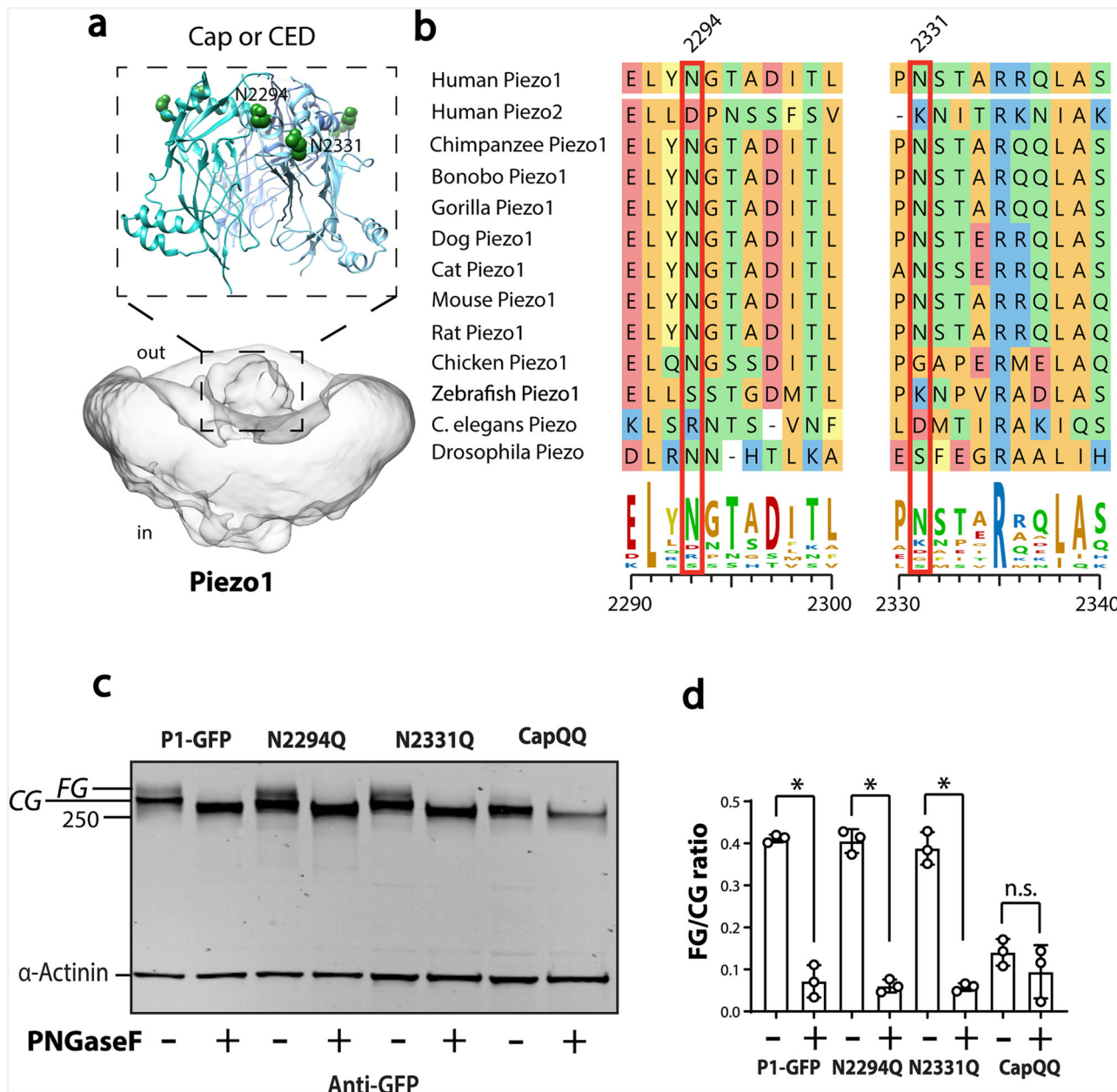
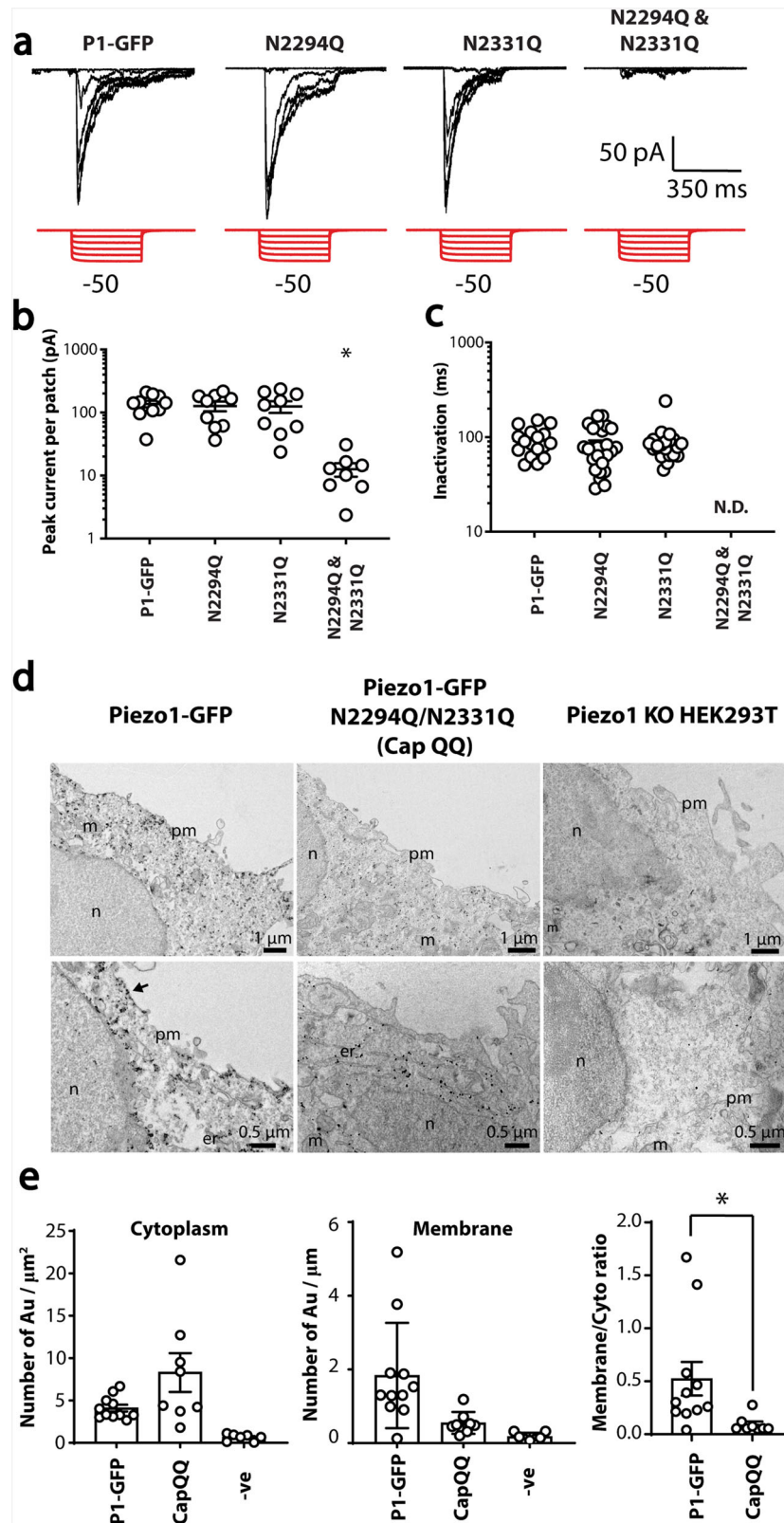


Fig. 3 Influence of Asparagine residues in the cap region of human Piezo1 on N-glycosylation. **a** Two asparagine residues present in the Cap domain of Piezo1. **b** Multiple sequence alignment illustrates these asparagine residues are highly conserved in Piezo1 homologues. **c** Representative blot showing the effect of PNGaseF treatment on lysate from HEK293 cells expressing Piezo1-GFP, N2294Q, N2331Q and N2294Q/N2331Q (CapQQ). **d** Quantification of the ratio [FG/CG] of the upper band (FG) and lower band (CG) with and without PNGaseF for Asn mutants in the Cap region. * $p < 0.05$ determined by Kruskal-Wallis test with Dunn’s post-hoc test.

We quantitatively compared the intensity of the upper fully glycosylated (FG) band with the lower core glycosylated (CG) band in replicate experiments (Fig. 3c, d). Comparison between PNGaseF treatment of WT, N2294Q, N2331Q showed patterns that suggested that the upper FG band was removed, and the size of the lower bands were reduced to the level of the unglycosylated form of the protein. In addition, western blots of the protein from the double mutant N2294Q/N2331Q showed no upper (fully glycosylated) band, while the lower core glycosylated protein was reduced in size. This finding suggested that core glycosylation also occurred in the N-terminal domain of Piezo1. This aligns with published findings on Piezo2 that show glycans in the propeller region⁴⁴.

The FG form of an ion channel often indicates the functional form, so we tested if changes in western blots correlated with electrophysiological analysis. A high-speed pressure clamp was used to apply negative pressure to cell-attached patches of transiently transfected Piezo1^{-/-} HEK293T cells. The two single mutants showed normal stretch-activated responses (Fig. 4a, b), which was consistent with two bands on western blots. Given strong evidence that the cap is involved in Piezo1 inactivation⁴⁵, we tested if inactivation was modified, but neither of the Asn to Gln mutants affected inactivation time constants in cell-attached patches (Fig. 4c). However, the N2294Q/N2331Q mutant had almost no stretch-activated current (Fig. 4a, b), which was consistent with the western blot pattern and indicated that the FG



Piezo1 protein represented the membrane protein pool (Figs. 2e, f and 3c).

From the patch-clamp data we could not rule out that N-glycosylation may also be required for stretch activation of Piezo1. The processing of N-glycans from high-mannose to higher molecular weight glycans (>2.5 kDa in size per glycan—termed complex or hybrid) requires the enzyme N-

acetylglucosaminyl-transferase I (GnT1, also known as MGAT1). Structural biologists have widely used HEK293S GnT1^{-/-} cells to restrict the heterogeneity introduced by N-linked glycosylation when attempting to determine structures using X-ray crystallography, and more recently Cryo-EM⁴⁶. As GnT1^{-/-} cells cannot process larger N-glycans (hybrid or complex), we asked two questions: (1) ‘Is the fully glycosylated species of human

Fig. 4 Effect of mutation of N2294 and N2331 on mechanically induced gating of Piezo1. **a** Electrophysiological recordings of HEK293T Piezo1^{-/-} expressing Piezo1-GFP, N2294, N2331Q and N2294Q/N2331Q in the cell-attached configuration in response to negative pressure applied using a high-speed pressure-clamp (red). **b** Quantification of peak current elicited per patch. **c** Quantification of inactivation of Piezo1-GFP, N2294, N2331Q and N2294Q/N2331Q from cell-attached recordings (ND—not determined). **d** Immunogold labelling using mouse monoclonal anti-Piezo1 primary antibody and electron microscopy of HEK293T Piezo1^{-/-} (KO) and cells expressing Piezo1-GFP and the CapQQ mutant (N2294Q/N2331Q)[pm plasma membrane, n nucleus, m mitochondria, er endoplasmic reticulum]. **e** Quantification of immunogold labelling in the cytoplasm (per μm^2), membrane (per μm) and the ratio of membrane to cytoplasmic labelling using immunogold comparing Piezo1 to the CapQQ mutant (N2294Q/N2331Q). * $p < 0.05$ determined using Mann-Whitney *U*-test.

Piezo1 present on western blots from lysates of GnT1^{-/-} cells? (2) ‘Can these cells support stretch induced gating of Piezo1 channels?’

First, Piezo1-GFP channels expressed in HEK293S GnT1^{-/-} cells presented as a single band on western blots consistent with the upper band being a glycosylated species containing large N-glycans (Supplementary Fig 5a). Piezo1-GFP also exhibited stretch-activated currents suggesting the larger N-glycans were not needed for stretch activation, however we do not know if they are required for activation in response to shear stress^{47,48}. Much like transient transfection in Piezo1^{-/-} HEK293T cells expression of the CapQQ mutant generated negligible stretch-activated currents when transiently transfected in HEK293S GnT1^{-/-} (Supplementary Fig 5b, c). Here, we should note that the residual current seen when transfecting the CapQQ (N2294Q/N2331Q) in HEK293S GnT1^{-/-} could have come from the endogenous Piezo1 in this cell type. The sensitivity of the stretch-activated currents of Piezo1-GFP was lower when expressed in HEK293S GnT1^{-/-} cells (Supplementary Fig 5d). The expression of Piezo1-GFP in GnT1^{-/-} cells suggested that larger N-glycans are not needed for stretch activation, and that only the core-glycans were ultimately necessary for transit through the Golgi to the plasma membrane.

To support the hypothesis that the double mutant (N2294Q/N2331Q) that lacked the larger molecular weight fully glycosylated protein was trafficking-defective we used radiometric Ca²⁺ imaging to explore the effect of Yoda-1 (2 μM) on Ca²⁺ influx. Fluorescence did not change in cells expressing the double mutant (N2294Q/N2331Q) on adding Yoda-1, thus indicating that the Ca²⁺ concentration did not rise (Supplementary Fig 6). These mutations do not reside near the putative Yoda-1 binding pocket so we surmised that they would be unlikely to influence Yoda-1 binding⁴⁹. Thus, the lack of a Yoda-1 response is congruent with no membrane localised Piezo1.

We confirmed the trafficking defect using nano-gold immunolabelling and transmission electron microscopy (TEM) in combination with Piezo1^{-/-} HEK293T cells. The micrographs clearly showed WT Piezo1 had reached the plasma membrane, while the N2294Q/N2331Q double mutant showed little or no membrane labelling (Fig. 4d). Quantification of the ratio of membrane versus intracellular nano-gold staining of Piezo1 and N2294Q/N2331Q showed a marked reduction in membrane labelling of N2294Q/N2331Q, which was consistent with a trafficking defect (Fig. 4e). Nano-gold labelling was not seen in un-transfected Piezo1^{-/-} HEK293T cells.

To corroborate the veracity of the antibody’s specificity, in addition to the western blots shown in Supplementary Figure 1, and immunogold negative controls (Fig. 4d: rightmost panels), immunofluorescence was used in combination with Piezo1-GFP expressed in Piezo1^{-/-} HEK293T cells. Supplementary Fig. 7 shows no staining of Piezo1^{-/-} HEK293T cells and more convincingly that un-transfected cells were not labelled. Moreover, we then corroborated the finding that N2294Q/N2331Q was trafficking defective using a similar strategy to previous work^{28,30,32,50} combining live cell labelling (Supplementary

Fig. 8), and a Piezo1 construct with an extracellular HA tag. Live cell labelling was only seen in cells expressing WT Piezo1 and not the N2294Q/N2331Q double mutant (Supplementary Fig. 8).

Piezo1 N-linked glycosylation in the propellers. To determine the location of N-linked glycosylation in Piezo1 channels use was made of a split human Piezo1 construct generated by the Gottlieb laboratory⁵¹. This construct has two portions of human Piezo1; the first extends from residue 1 to 1591 fused to mCherry (N-terminal portion—propellers), and the second starts with GFP that is fused to residue 1592 and extends to residue 2521 (C-terminal portion—pore and cap) (Fig. 5a). Western blotting showed that this construct was expressed as two separate molecular entities smaller in size than WT Piezo1 (Fig. 5b and Supplementary Fig 9).

The size of the C-terminal portion of the split protein (Fig. 5b; shown in green) was minimally affected by PNGaseF treatment (~5 kDa), the size of which was indicative of 1–2 core glycans (~2–5 kDa). Instead, the larger glycan appeared to be present on the N-terminal portion of the protein (Fig. 5b, c). The N-terminal portion (coloured red) migrated as two bands. The larger more diffuse band was abolished and the lower band reduced in size on treatment with PNGaseF (Fig. 5b).

The N2294Q/N2331Q double mutant of the split construct gave a C-terminal domain that was unaffected by PNGaseF treatment again indicating that it was un-glycosylated; but the N-terminal portion had no larger glycosylated species (Fig. 5b, white box). Thus, the two Asn residues in the cap appeared to determine the glycosylation status of the propeller asparagines. The larger glycosylated species of the N-terminal fragment was also ablated by incubation with brefeldin A (Supplementary Fig. 10a). This is consistent with the split protein being processed in a similar fashion to the full-length Piezo1 (Fig. 1i).

The WT split protein produced stretch-activated current when expressed in Piezo1^{-/-} HEK293T cells, while the double mutant (N2294Q and N2331Q) did not (Fig. 5d, e). As a means of providing further supporting evidence for core glycans being added to Piezo1 at both N2294 and N2331, we made single mutants of the same split construct and compared the molecular size to the split WT and double mutant (N2294Q and N2331Q). The corresponding blot showed a similar size between the single mutants (Fig. 5f). The size was less than that of WT but larger than the double mutant, further suggesting that both asparagines were glycosylated (Fig. 5f).

The split construct that produced smaller Piezo1 protein fragments was used to determine, if the propeller domains contained Asn residues that has larger N-glycans added. There are six residues that are possibilities to undergo N-linked glycosylation in the N-terminus of human Piezo1: N295, N658, N885, N892, N1095 and N1222. Of these, five out of the six are in extracellular loops while one (N1222) is part of a transmembrane helix, so it was not explored further. Single Asn to Gln mutations were made to prevent N-linked glycosylation in the split construct. Again, the CapQQ (N2294Q and N2331Q) mutant

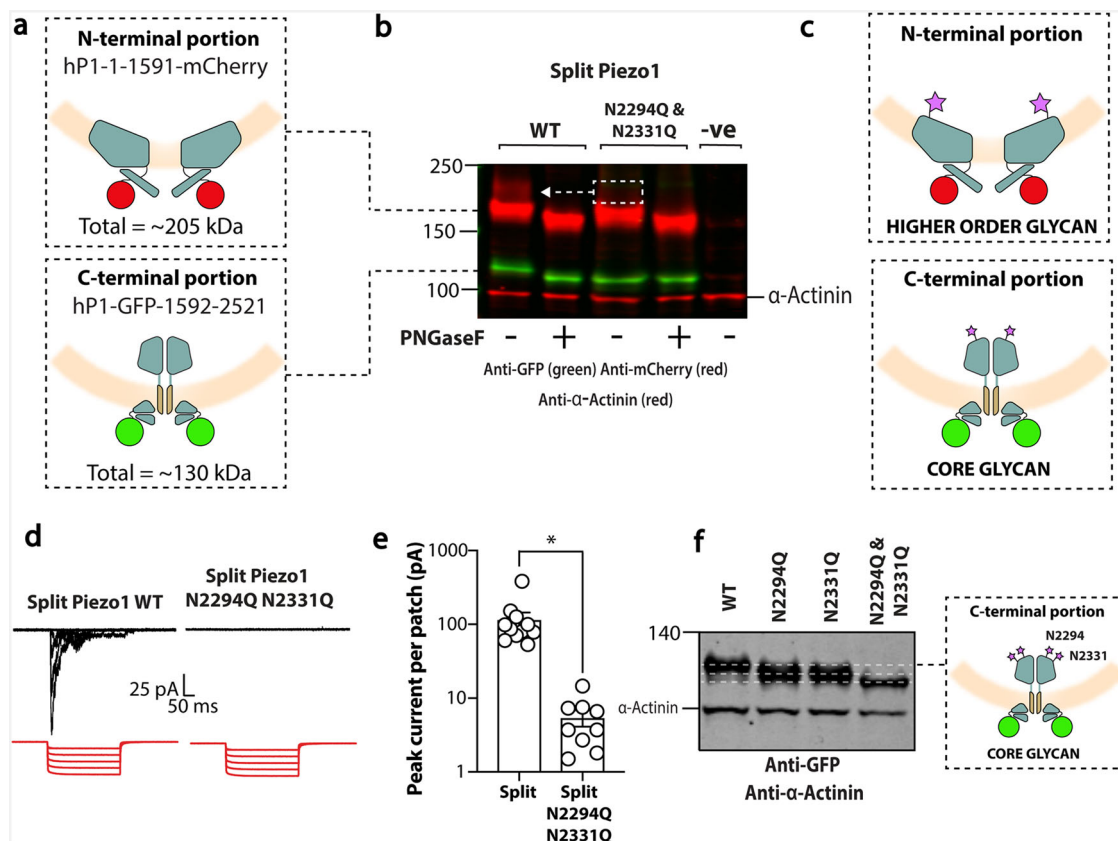


Fig. 5 N-glycosylation of Piezo1 in a split construct. **a** Diagram depicting the human split Piezo1 protein. **b** Representative blot showing the split human Piezo1 protein and the split human Piezo1 protein with the double cap mutant N2294Q and N2331Q with and without PNGaseF treatment. **c** Diagram illustrating where glycans are likely to be located. **d** Electrophysiological recordings of Piezo1^{-/-} HEK293T cells expressing human split Piezo1 and the double cap mutant N2294Q and N2331Q in the cell-attached configuration in response to negative pressure applied using a high-speed pressure-clamp (red). **e** Quantification of peak current elicited per patch. **f** Representative blot showing the C-terminal portion of the split human Piezo1 protein and the mutants N2294Q, N2331Q and N2294Q/N2331Q. Note that the single mutants run at the same size but the double mutant is smaller. **p* < 0.05 determined by Mann-Whitney *U*-test. -ve represents an un-transfected control.

had a smaller C-terminal fragment that was concluded to be due to a lack of core-glycans in the cap; and N885Q had limited evidence of glycosylation on their N-terminal fragments despite containing the two critical Asn residues in the cap (Supplementary Fig. 10b).

Subsequently, constructs of full-length Piezo1 were made in which all five Asn residues were mutated to Gln. Stretch activated currents were measured for each of these full length Piezo1 variants (Fig. 6a). Figure 6a shows the peak currents of cell-attached patches when these mutants were expressed in Piezo1^{-/-} HEK293T cells. Specifically, there was a large reduction in stretch activated currents in N885Q; and western blotting confirmed an almost complete loss of the larger N-glycosylated species in this single mutant (Fig. 6c and Supplementary Fig. 11). None of the five mutations altered unitary conductance from WT (47 ± 2 pS; *n* = 5) (Supplementary Fig. 12).

We noted that the glycosylation of N658Q was different as the patch clamp data showed a mild reduction in stretch-activated currents (Fig. 6b). Based on these findings combinations of Asn to Gln mutants were constructed.

A double mutant of N295Q and N885Q gave stretch-activated responses that largely followed the current generated from the single N885Q mutant; while a combination of N658Q and N885Q further reduced the stretch activated current (Fig. 6d, e). Combining all five N-terminal Asn residues to Gln mutants (N295Q, N658Q, N885Q, N892Q, N1095Q), or all seven Asn residues subjected to electrophysiological analysis in this study

(N295Q, N658Q, N885Q, N892Q, N1095Q, N2294Q, N2331Q) resulted in maximum currents that fell to almost zero in response to negative pressure pulses (Fig. 6e). The construct harbouring seven Asn to Gln (7N-Q) mutations did not reach the plasma membrane as assessed using immunogold labelling in a manner similar to that seen with the CapQQ (N2294Q/N2331Q) in Fig. 3.

Western blot analysis of the double mutants, particularly N658Q and N885Q showed an almost complete loss of the larger N-glycosylated species in a manner similar to the CapQQ (N2294Q/N2331Q) (Fig. 6g). The 5N-Q (N295Q, N658Q, N885Q, N892Q, N1095Q) and 7N-Q (N295Q, N658Q, N885Q, N892Q, N1095Q, N2294Q, N2331Q) mutants on western blots had bands that were consistent with full-length protein, but there was a complete lack of the upper fully glycosylated species (Fig. 6h). Moreover, the lower band in both the 5N-Q and 7N-Q Piezo1 mutants were smaller than that of the core-glycosylated Piezo1-GFP. The 7N-Q mutant also displayed lower protein levels indicative of reduced stability. This finding was consistent with the lack of core-glycans being attached at these sites. As final evidence that all the N-linked glycans were removed from the 7N-Q mutant, we treated it with PNGaseF and saw that it had no effect on protein size (Fig. 6i).

Lack of larger N-glycosylated species in trafficking defective Piezo1 mutants. As the data above suggested that the presence of the larger N-glycosylated species was a surrogate for normal membrane trafficking in human Piezo1 channels, we investigated

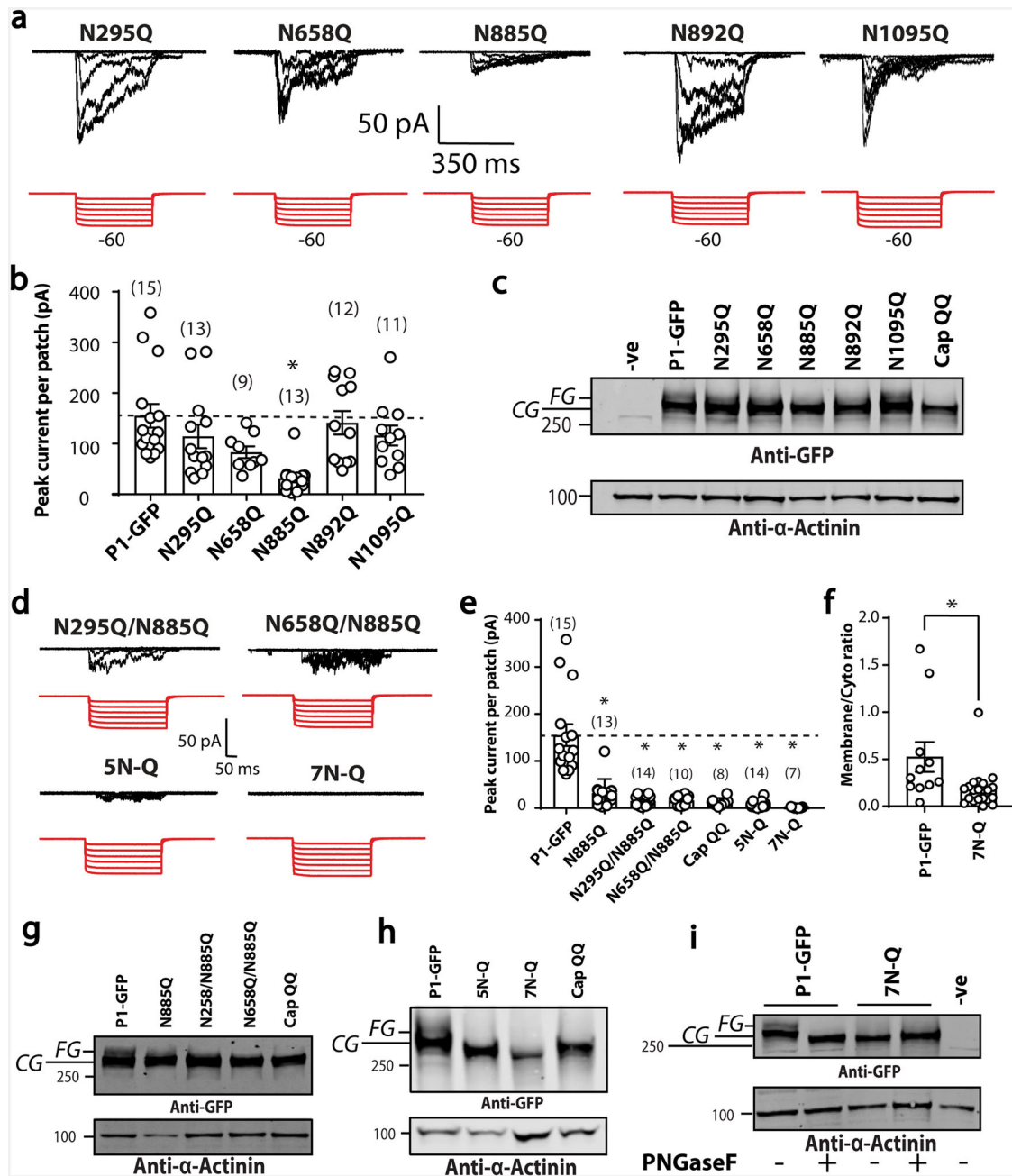


Fig. 6 N-glycosylation in the N-terminus of Piezo1. **a** Electrophysiological recordings of Piezo1^{-/-} HEK293T expressing single Asn to Gln Piezo1-GFP mutations in the N-terminus (N295Q, N658Q, N885Q, N892Q, N1095Q) in the cell-attached configuration in response to negative pressure applied using a high-speed pressure-clamp (red). **b** Quantification of peak current elicited per patch for point mutations shown in **a** compared to current from Piezo1-GFP. **c** Representative western blot of all Asn to Gln mutants in the N-terminus of Piezo1 compared to the double mutant in the Cap region (CapQQ). **d** Electrophysiological recordings of HEK293T Piezo1^{-/-} expressing Piezo1 with multiple Asn to Gln mutations (as indicated) in the cell-attached configuration in response to negative pressure applied using a high-speed pressure-clamp (red). [5N-Q—N295Q, N658Q, N885Q, N892Q, N1095Q and 7N-Q—N295Q, N658Q, N885Q, N892Q, N1095Q, N2294Q, N2331Q]. **e** Quantification of peak current elicited per patch for mutation combinations shown in **d** compared to current from Piezo1-GFP, N885Q and CapQQ. **f** Membrane to cytoplasmic ratio of immunogold labelling of the 7N-Q mutation compared to human Piezo1. **g** Representative western blot showing the comparison between Asn to Gln mutations of single and double mutations illustrating the strong impact of N885Q mutation on the upper FG band of Piezo1 heterologously expressed in Piezo1^{-/-} HEK293T. **h** Representative blot showing the comparison between multiple Asn to Gln mutations 5N-Q, 7N-Q and the CapQQ (N2294Q/N2331Q). **i** Representative blot showing the comparison between PNGaseF digested WT and the 7N-Q mutant. **p* < 0.05 determined by Kruskal-Wallis test with Dunn's post-hoc test or Mann-Whitney *U*-test. -ve represents an un-transfected control.

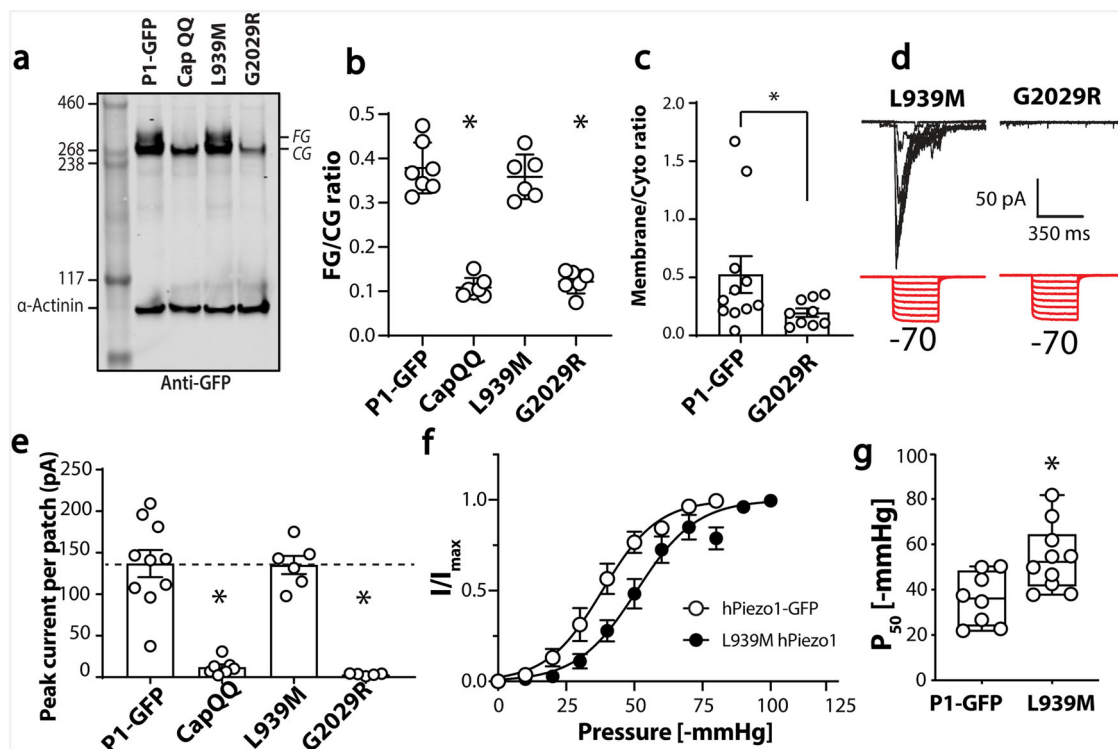


Fig. 7 N-glycosylation status of Piezo1 variants linked to generalised lymphatic dysplasia (GLD). **a** Representative western blot showing Piezo1 protein, CapQQ (N2294Q/N2331Q) and two GLD associated mutations (L939M and G2029R). **b** Relative quantification of intensity of upper band (FG) over lower band (CG) for Piezo1, CapQQ, L939M and G2029R. **c** Membrane to cytoplasmic ratio of immunogold of G2029R compared to human Piezo1. **d** Electrophysiological recordings of Piezo1^{-/-} HEK293T expressing L939M and G2029R in the cell attached configuration in response to negative pressure applied using a high-speed pressure-clamp (red). **e** Quantification of peak current elicited per patch for point mutations shown in **d** compared to current from Piezo1-GFP and CapQQ mutant. **f** Pressure response curve for Piezo1-GFP against L939M expressed in Piezo1^{-/-} HEK293T. **g** Minimum to maximum box and whiskers plot showing the average P_{50} [-mmHg] of Piezo1-GFP and L939M variant.

if disease-linked variants were identifiable by using this approach. Such an approach has been extensively used in studies of loss-of-function disease-causing variants in *KCNH2* that cause LQTS¹⁸. First, variants linked to generalised lymphatic dysplasia (L939M²⁷ and G2029R²⁸) were studied.

Much like the Cap QQ (N2294Q/N2331Q) mutant, G2029R shows no signs of N-glycosylation (Fig. 7a). In comparison, L939M western blots appeared similar to those of the WT, with two bands. The relative amounts were quantified using the intensity of the upper band (fully glycosylated, FG) versus that of the lower band (core glycosylated, CG), and these showed a marked reduction of the FG band in the Cap QQ (N2294Q/N2331Q) and the G2029R mutants (Fig. 7b). The latter mutant had already been convincingly shown with immunofluorescence to be trafficking-defective²⁸, a fact we confirmed here using immunogold electron microscopy (Fig. 7c). In whole-cell mode, previous work suggests G2029R exhibits small indentation evoked currents²⁸ congruent with the small level of immunogold labelling we observe. However, when surveying a smaller portion of the membrane using cell-attached patch clamping, we record little to no stretch-activated current in cells expressing G2029R in comparison to L939M in which peak currents were comparable to WT (Fig. 7d, e). This finding provided further support for the idea that the presence of larger N-glycosylated species of Piezo1 is indicative of normal membrane trafficking.

While the maximum stretch-activated L939M currents were comparable to WT, they did show a modest rightward shift in the pressure-response curve (Fig. 7f, g). It is important to note that we were not aiming to definitively ascribe disease causation to L939M, in fact, the patient with this mutation also had other

missense variants reported in Piezo1 (F2458L, R2456C), which we did not test²⁷. What was evident was that WT and L939M Piezo1 both showed a double band on a western blot, and they gave stretch activated currents; and both CapQQ and G2029R only had the lower band in the western blots and gave limited stretch activated currents.

Given that we could clearly distinguish a trafficking defective human Piezo1 variant (G2029R) from WT or a variant that reaches the plasma membrane (L939M), we posit that this experiment could serve as an assay for ameliorated trafficking.

Temperature effects on trafficking. Again, using parallels with the $K_{v11.1}$ and CFTR literature, we attempted to rescue aberrant trafficking using two methods. The first was low temperature treatment, and the second was a pharmacological approach^{18,22,52,53}. Specifically, a cohort of $K_{v11.1}$ and CFTR variants could be rescued at low temperature (<30 °C), which is thought to improve protein folding and hence trafficking. The same experimental protocol was used for the Piezo1 variants, expressed in HEK293 cells for 24 h at 27 °C. WT $K_{v11.1}$ was used with a temperature rescuable mutant A422T as a positive control. Twenty-four hours at 27 °C increased the amount of fully glycosylated $K_{v11.1}$ A422T, which was consistent with previous reports (Supplementary Fig. 13a, b). With the same protocol for Piezo1 the density of the upper band in the western blot of the G2029R mutant was not increased. Furthermore, the treatment reduced the upper band of WT and L939M suggesting amelioration of trafficking (Supplementary Fig. 13c). The lower membrane expression level was confirmed by using patch clamp experiments (Supplementary Fig. 13d). Importantly, all patch

clamp experiments were carried out at room temperature as previous reports suggested that Piezo1 activity is temperature dependent⁵⁴. These findings provided further evidence that the intensity of the upper band in western blots of the HEK Piezo1 proteins reported on channel trafficking to the plasma membrane.

Drug effects on trafficking. $K_{v11.1}$ is stabilised by the channel blocker E4031, which improves membrane trafficking²². So, we tested if the antagonist of Yoda-1 activation Dooku-1⁵⁵ offers the same type of chaperone effect on Piezo1. Also, if Dooku-1 did not inhibit stretch-activation of Piezo1, this type of molecule might be used therapeutically if it could improve trafficking.

Treatment of HEK cells for 48 h with 5 μ M Dooku-1 (higher concentrations could not be attained due to its low solubility) did not improve the intensity of the upper western blot FG band of the WT, L939M or the G2029R mutant of Piezo1 (Supplementary Fig. 13e). In the process of confirming this outcome with patch clamp analysis, the current per patch of Piezo1 was seen to be reduced by 30–60% (Supplementary Fig. 13f). After washout, peak currents per patch returned to >80% of untreated levels. This suggested that Dooku-1 perturbed Piezo1 stretch-activation. Therefore, we tested acute addition of 5 μ M Dooku-1. Indeed, it reduced stretch activation by ~50%, which was largely reversed on washout.

This warrants further study. While neither temperature nor Dooku-1 could reverse amelioration of trafficking this does provide the basis for future studies to look at a wider range of loss-of-function Piezo1 mutants. However, it was first necessary to see if modified N-glycosylation was applicable to other reported disease-linked Piezo1 variants.

Co-expression of trafficking defective Piezo1 mutants. Heterozygous Piezo1 missense variants have been linked to disease. To broaden the relevance of our data, we investigated more variants with genetic loci that are linked to bicuspid aortic valve (BAV)²⁹, and examined how co-expression of disease-linked variants with WT Piezo1 might affect Piezo1 activity. First, WT Piezo1-GFP was co-expressed with equivalent amounts of DNA of L939M and G2029R. The stretch activated currents elicited by negative pressure application from a high-speed pressure clamp (Supplementary Fig. 14a) were recorded followed by the variants at loci linked to BAV (Supplementary Fig. 14b–d). Co-expression of S217L, Y2022A and G2029R with Piezo1-GFP had a large effect on the stretch evoked currents (Supplementary Fig. 14a–c). The stretch evoked activity was seen to be correlated with the extent of fully glycosylated protein, as seen for L939M and G2029R (Fig. 7a, b). Consistent with all the previous data, G2029R, S217L showed a reduced upper FG band in the western blot (Supplementary Fig. 14e). Moreover, co-expression of the G2029R, S217L mutant with the WT protein also reduced the FG band compared with the control (Supplementary Fig. 14e–g). This finding follows the maximal amount of current elicited from cell-attached patches and suggested a dominant-negative effect (Supplementary Fig. 14h).

We could not guarantee that 100% of the cells were transfected with both WT and mutant protein DNA as they were both GFP fused. However, the patch clamp observations shown in Fig. 8 were seen to be consistent by co-expressing a GFP fused Piezo1 with mCherry fused mutant proteins (Fig. 8 and Supplementary Fig. 14i). This allowed us to select only cells that were expressing both fused proteins for electrophysiological analysis; almost identical current patterns were recorded (Supplementary Fig. 14i) to those of the maximal current data shown in SI Fig 14h.

As final evidence that some mutants displayed a dominant-negative effect we focussed on the S217L mutant. Western blots of

this mutant had a single band with little sign of the higher molecular weight fully glycosylated species, regardless of the cell type in which it was expressed (Fig. 8a and Supplementary Fig. 15). Western blots on cell lysate from Piezo1^{-/-} HEK293T co-transfected with every combination of WT and S217L-GFP and -mCherry fused proteins are shown in Fig. 8b. Both S217L-GFP and -mCherry fused Piezo1 showed a single band with elimination of the band corresponding to the glycosylated species of the co-transfected wild-type protein (Fig. 8b). The lack of fully glycosylated species correlated well with the stretch evoked current (Fig. 8c) and TIRF microscopy showed little membrane localisation of the S217L mutant (Supplementary Fig. 16).

Discussion

Post-translational modification is critical for function and localisation of transmembrane proteins. N-linked glycosylation is one of the most frequently encountered and heterogeneous forms of co-translational and post-translational modification. Here, we showed that the mechanically-gated ion channel Piezo1 underwent N-linked glycosylation and migrated as a doublet on a western blot similar to other ion channel proteins like $K_{v11.1}$ ^{18,25}. This double band appearance on western blots was not dependent on the nature of the molecular tag attached to it. The fully glycosylated species was evident in GFP tagged proteins (C-terminal or 1591 position), mCherry tagged proteins (1591 position), mouse Piezo1 fused to TdTomato and un-tagged natively expressed Piezo1 in fibroblasts.

By using PNGaseF, which specifically cleaves N-linked oligosaccharides, the upper band of human Piezo1 was found to be heavily N-glycosylated (~25 kDa). Treatment with a mixture of deglycosylases produced a similar effect on western blots implying that the upper band species was unlikely to contain significant amounts of cleavable O-linked oligosaccharides. This was supported using GnT1^{-/-} HEK293S cells. Unlike most cell types, this cell has a genetic deletion that prevents the processing of larger N-glycans (complex and hybrid). Western blots from lysates of these cells also lacked an upper band. Using brefeldin A treatment, which indirectly inhibits transport between the ER and Golgi ultimately resulting in proteins being retained in the ER^{36,56–58}, we showed unsurprisingly that the larger N-glycans must be processed in the Golgi.

In other ion channel proteins, the fully glycosylated protein (upper band) has been used as an indicator of normal membrane trafficking, whereas the core glycosylated protein (lower band) largely represents the immature version present mainly in the ER and Golgi^{18,22,59}. Consistent with this knowledge, using unroofed fibroblasts and biotinylation, we showed that the N-glycosylated version of natively expressed Piezo1 constituted the major component of the membrane pool of Piezo1. In RBCs only a single Piezo1 band was evident in western blots and the single band size was reduced on PNGaseF treatment. This finding was consistent with the lack of ER and Golgi in mature RBCs.

The larger N-glycosylated species of Piezo1 was dependent on two critical Asn sites in the cap region (Fig. 9). Which of these two asparagines that became glycosylated seemed of little consequence as single mutants (N2294Q or N2331Q) could still traffic and produce mechanically evoked currents. A previous mass spectrometry study suggested at least one of these two Asn residues in Piezo1 was glycosylated⁴³, which is consistent with a Cryo-EM structure of Piezo2 where one glycosylated asparagine was resolved in the cap⁴⁴. When both residues were ablated (N2294Q and N2331Q) little to no current was present in electrophysiological experiments; and the protein lacked the higher molecular weight band indicative of a protein with larger N-glycans. Interestingly, PNGaseF reduced the size of the core

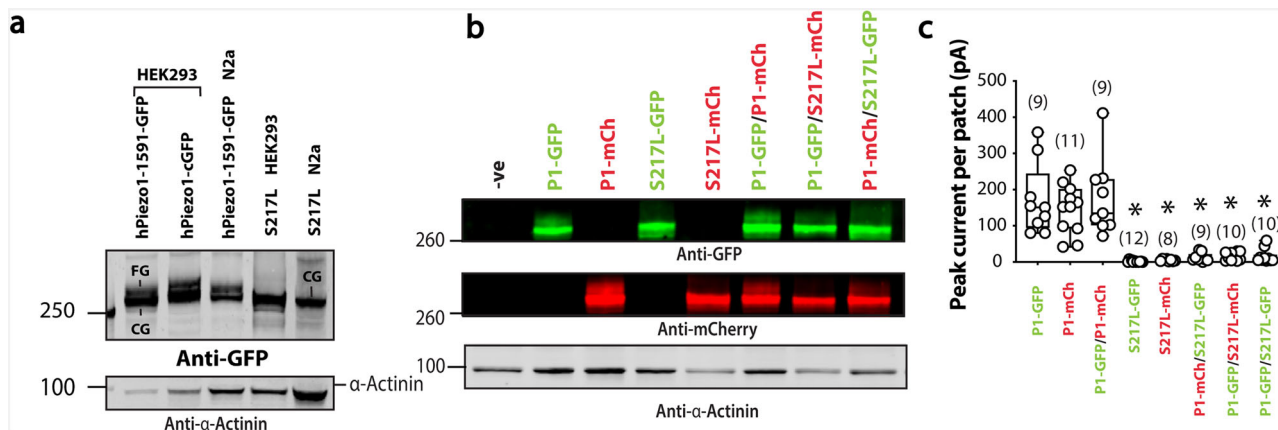


Fig. 8 Comprehensive analysis of co-expression of S217L Piezo1 and WT Piezo1 fused to GFP and mCherry. **a** Representative western blot of Piezo1-GFP and S217L expressed in HEK293 and Neuro2a cells (N2a). **b** Representative western blot of Piezo1-GFP, Piezo1mCherry, S217L-GFP, S217L-mCherry, and co-expression of Piezo1-GFP/Piezo1-mCherry, Piezo1-GFP/S217L-mCherry, Piezo1-mCherry/S217L-GFP. The GFP and mCherry signal are shown separately. **c** Quantification of peak current elicited per patch of all combinations expressed in Piezo1^{-/-} HEK293T cells. Asterisk (*) denotes statistical significance $p < 0.05$ determined by Kruskal-Wallis test with Dunn’s post-hoc test.

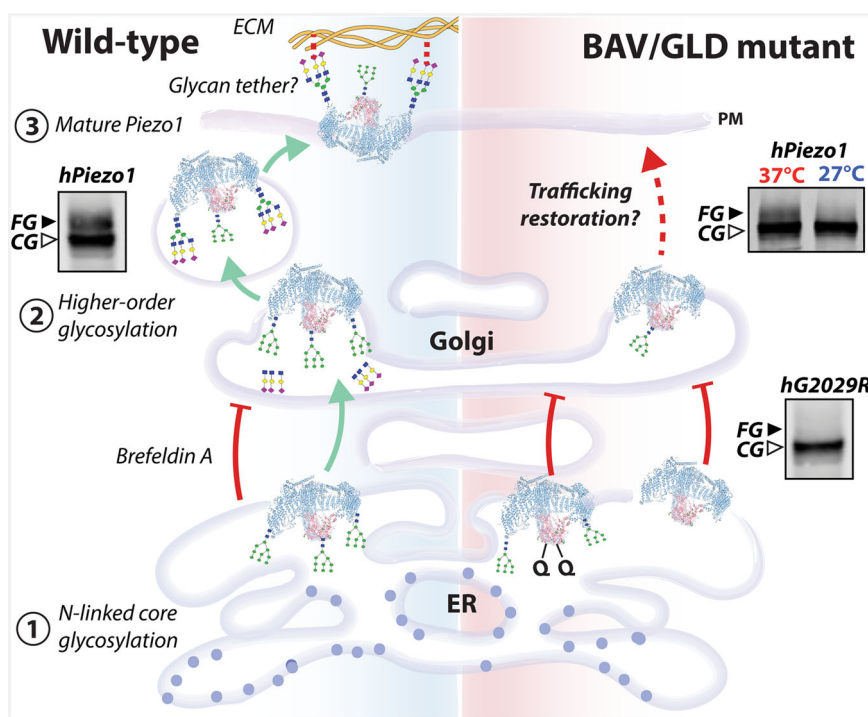


Fig. 9 Summary of Piezo1 biosynthetic pathway. Core-glycans added in the cap (N2294/N2331) while folding in the ER are critical for the larger N-glycans in the propeller (primarily at N885) which are processed in the Golgi. Aberration of glycosylation reflects impaired trafficking, and perhaps the larger glycans may act as molecular tethers linking to the ECM as suggested for ENaC⁷⁰. Summary adapted from Kanner et al.⁶⁰.

glycosylated N2294Q/N2331Q double mutant protein, thus indicating that other sites also undergo N-linked glycosylation.

Using a split Piezo1 protein, we showed that both Asn residues became glycosylated and indeed that these residues dictated N-glycosylation in the propeller regions. Of the six sites predicted to undergo N-glycosylation in the propellers, we identified two crucial residues in the N-terminus that are the sites of larger N-glycans (N658 and N885). The analogous residues to N658 and N885 in mouse Piezo1 are present in two loops that were previously identified by the Xiao laboratory to be essential for mouse Piezo1 function; and in electrophysiological stretch assays they gave minimal current consistent with our results³².

Thus, our data suggested that the lack of a higher molecular weight species on a western blot, as seen with the double mutant (N2294Q/N2331Q), indicates aberrant trafficking of Piezo1. This mirrors perfectly what has been reported with $K_{v11.1}$ and CFTR channels¹⁸. Ultimately it is core N-glycosylation in the cap and propellers that are necessary for trafficking, as current can still be produced in specialised GnT1^{-/-} cells that cannot process larger N-glycans (although they can produce lower molecular weight oligomannose glycans). In all cells expressing GnT1 that we have tested, such processing in the ER and Golgi results in larger amounts of N-glycosylation and the upper band on a western blot.

Probing N-glycosylation status in this manner provides a rapid and reliable method to determine if human Piezo1 variants, that are generated for structure-function studies³³ or in studies of disease-linked variants, exhibit aberrant trafficking exemplified by our data on G2029R, a known trafficking defective Piezo1 variant²⁸. We also used glycosylation status to attempt to rescue G2029R using two widely used strategies; low temperature treatment and a pharmacological chaperone²². Neither aided G2029R trafficking; but for $K_{v11.1}$ channels only a subset of mutants could be rescued²² by the respective treatments. Nevertheless, it is plausible that Piezo1 mutants may be rescuable using alternative approaches⁶⁰ or pharmacological chaperones.

N-glycosylation status can also be used in co-expression studies to interrogate the impact of disease-linked variants on the WT protein, thus mimicking heterozygosity. Here, we provide evidence that some Piezo1 variants had a dominant negative effect as they reduced WT function. The most notable example of this was S217L. Its effect was very similar to that of dominant negative mutants such as A561V on the trafficking of the $K_{v11.1}$ channel⁶¹. While there was no guarantee that every cell was expressing exactly the same quantity of mutant and WT Piezo1 proteins, as would be in the case in vivo, the data from western blots and patch clamp analysis were consistent with a dominant negative effect. This was congruent with the fact that the higher molecular weight species (the FG Piezo1 protein) was indicative of the functional membrane protein pool.

While we concluded that the latter mutants are aberrantly trafficked, we could not rule out the fact that additional disease-causing mechanisms such as reduced stability or gating phenotypes (particularly for S217L²⁹) existed. However, our data demonstrated that trafficking deficient Piezo1 mutants were differentially processed in heterologous expression systems as seen in the extensive studies of $K_{v11.1}$ ^{18,52,62–65} and CFTR^{20,66,67}.

We have described this larger species evident on western blots as the ‘fully glycosylated’ protein. The larger species could have complex or hybrid N-glycans¹⁵. The exact composition of the glycans is beyond the scope of this study. However, it is likely of interest going forward when trying to decipher whether these glycans may interact with the extracellular matrix and function as molecular tethers^{68,69} responding to shear stress as suggested for the epithelial sodium channel (Fig. 9)⁷⁰. The glycans may also facilitate interactions with binding partners such as PECAM1⁷¹ or E-cadherin⁷² or with specific lipids such as glycolipids⁷³, which could modify the channel’s ability to sense membrane tension⁷⁴.

In integrins, N-glycans are important for clustering. Hence, future studies could explore whether Piezo1 N-glycosylation is involved in the previously identified clustering of Piezo1 in the plasma membrane⁹. If N-glycans are a means of interactions with other membrane proteins, or the ECM⁷⁰, this gives cells an extra dynamic mechanism to regulate mechanosensitivity. This may explain the differential sensitivity to applied force seen when Piezo1 was expressed in HEK293S GnT1^{-/-} cells that cannot process larger N-glycans. As previously mentioned for G2029R and S217L, we cannot rule out the fact that these mutations and/or the resulting loss of N-glycosylation may also alter tension sensitivity (or their response to shear stress), and further work should aim to interrogate the involvement of N-glycans in Piezo1 mechanosensitivity.

In conclusion, we have shown that the fully glycosylated version of Piezo1 in vitro is indicative of the mature species, which is localised to the plasma membrane. Thus N-glycosylation status will be valuable in studies of disease-linked variants of Piezo1; and the cell-biological protocols developed here could provide an analytical platform for identifying molecular chaperones to be used in the clinical treatment of Piezo1 trafficking defective variants.

Methods

Cell lines. Piezo1^{-/-} HEK293T cells²⁸ were a gift from Dr Ardem Patapoutian (The Scripps Research Institute, La Jolla, CA, USA); HEK293 (R78007, Scientific, Waltham, MA, USA) was a gift from Dr Nicola Smith (UNSW, Sydney, NSW, Australia); HEK293S GnT1^{-/-} cells were a gift from Dr Jamie Vandenberg (VCCRI, Sydney, NSW, Australia); and human BJ-5ta-hTERT foreskin fibroblasts were provided by Dr. Michael Sheetz (UTMB, Galveston, TX, USA). Cell lines were not authenticated and were not listed in the database of commonly mis-identified cell lines maintained by ICLAC (<http://iclac.org>) and NCBI Biosample (<http://www.ncbi.nlm.nih.gov/biosample>). All cell lines were confirmed to be mycoplasma free.

Mutagenesis. Site-directed mutagenesis of human and mouse Piezo1 was undertaken using a custom protocol with the high-fidelity polymerase PfuUltra. The mouse C-terminal GFP fusion construct was generated by deleting the IRES sequence using site-directed mutagenesis from the pcDNA3.1 IRES GFP construct of mouse Piezo1 (Provided by Dr Ardem Patapoutian). Primers for point mutations and fusion protein generation are listed in Table 1.

Western blotting. Cells were cultured in Dulbecco’s modified Eagle medium (DMEM; Sigma-Aldrich, St. Louis, MO, USA) supplemented with 10% v/v foetal bovine serum (ThermoFisher Scientific, Waltham, MA, USA) and incubated at 37 °C with 5% CO₂. GFP or mCherry-fused WT and mutant human Piezo1 cloned from HEK cells⁷⁵, or GFP-fused mouse Piezo1 were transfected into HEK293T Piezo1^{-/-} cells, HEK293S GnT1^{-/-} or HEK293 cells (ThermoFisher Scientific, Cat. No. R78007) using Lipofectamine 3000 transfection reagent (ThermoFisher Scientific) with 800 ng of DNA (400 ng WT and mutants, respectively, for co-expression transfection). The medium was changed 24 h after transfection. Cells were harvested 72 h after transfection and solubilized in radio-immunoprecipitation assay buffer (RIPA) buffer [Tris buffer 10 mM, ethylenediaminetetraacetic acid (EDTA) 1 mM, NaCl 140 mM, in (% w/v): Sodium deoxycholate 0.1, SDS 0.1, Triton X-100 1.0, pH 7.2] supplemented with 1 × EDTA-free protease inhibitor cocktail tablets (Sigma-Aldrich), 1 mM (phenylmethylsulfonyl fluoride) PMSF, 2 mM tris(2-carboxyethyl)phosphine (TCEP), and 1 mM N-ethylmaleimide (NEM) for 10 min on a rotating wheel at 4 °C. Cell lysates were cleared by centrifugation at 13,000×g at 4 °C for 20 min. Transfection efficiency was estimated, and the relative Piezo1 concentration was determined from the intensity of fluorescence of the lysate using a PHERAstarFS microplate reader (BMG

Table 1 Primers used for site directed mutagenesis in this study.

| Primer | Sequence |
|------------------------------|--------------------------------------|
| hP1-N2294Q Sense: | gcgggagctctaccagggcagcggccgaca |
| hP1-N2294Q Anti-sense: | tgtcggccgtgccctgtagagctcccgc |
| hP1-N2331Q Sense: | ggccctggccctcagagcactgcacgg |
| hP1-N2331Q Anti-sense: | ccgtgactgctctgaggggcccagggcc |
| hP1-L939M Sense: | tggcctcgaataaccatcagcagcacttg |
| hP1-L939M Anti-sense: | caagtgcctgctgatgattcaggagcca |
| hP1-G2029R Sense: | aagccagcttgcgacgacggctctg |
| hP1-G2029R Anti-sense: | caagaccgtgctgcgaagctggcctt |
| hP1-S217L Sense: | catcgccacccttggccctctc |
| hP1-S217L Anti-sense: | gagagggcccaaggggtggcgatg |
| hP1-Y2022A Sense: | tgaccgcgccctgcctgcgcaagacc |
| hP1-Y2022A Anti-sense: | ggtcttgcgaggcagggcgccgctca |
| hP1-K2502R Sense: | ggtagaggaagatgagcctggctacaactct |
| hP1-K2502R Anti-sense: | ggaggagttgatgcccaggtcattctctac |
| hP1_N295Q_Sense | cgtgggctggagcactgggtgggacc |
| hP1_N295Q_Anti-sense | cttcgtgggtcccaccagtgctccagcc |
| hP1_N658Q_Sense | gtgaagccagtgcctggccagtaggcag |
| hP1_N658Q_Anti-sense | ctgcctactggccagctcactgcttcac |
| hP1_N885Q_Sense | gaagggctcggctgactggctggaatactctg |
| hP1_N885Q_Anti-sense | caggagtattccagcagtgaccgagcccttc |
| hP1_N892Q_Sense | gcaagttggtcctctgggggagggctcgg |
| hP1_N892Q_Anti-sense | gccctccccagagcaccactgtctgcc |
| hP1_N1095Q_Sense | gaggttgggtgactgggggcccggagg |
| hP1_N1095Q_Anti-sense | cttcggggccccagtcaccaacctc |
| hP1_N1222Q_Sense | ggagatgatgacggctgactgacagaatgagcagct |
| hP1_N1222Q_Anti-Sense | gactgcctattctgtaccagtgaccgtcatctcc |
| mP1_Ct_GFP fusion-Sense | tggacacgtgagagggagacaaccatggtgagcag |
| mP1_Ct_GFP fusion-Anti-sense | cttctcaccatggtgtctcctctcagctgtcca |

LABTECH, Ortenberg, Germany). For PNGaseF (peptide N-glycosidase F, EC 3.5.1.52) digestion, 5% v/v PNGaseF (New England Biolabs, Ipswich, MA, USA) and 50 mM NEM were added to lysates mixed with 1× GlycoBuffer and incubated on ice for 1 h. For comparison Protein Deglycosylation Mix II P6044 (NEB) was also used with an identical protocol. Lysates that were undigested or digested were then mixed with SDS-PAGE sample buffer and loaded and run on a 3–8% Tris-Acetate gel (Thermo Fisher Scientific) before being transferred to a nitrocellulose membrane (Bio-Rad, Hercules, CA, USA). For quantitative western blot analysis, GFP-fused Piezo1 was probed with a rabbit monoclonal anti-GFP antibody (Santa Cruz Biotechnology, Dallas, TX, USA; 1:5000 dilution); mCherry-fused Piezo1 protein was probed with rat monoclonal anti-mCherry antibody (Clone 16D7, ThermoFisher Scientific; 1:1000 dilution); the native human Piezo1 channel was probed using a mouse monoclonal anti-Piezo1 antibody (Cat# NBP2-75617, Novus Biologicals, Centennial, CO, USA; 1:1000 dilution); mouse anti- α -actinin antibody (Santa Cruz Biotechnology; 1:5000 dilution) or anti- α -tubulin (Clone DM1A, Sigma Aldrich, T9026) antibody was added simultaneously for a loading comparison followed by anti-rabbit IRDye680 at 1:20,000, anti-rat IRDye800 at 1:10,000 and anti-mouse IRDye800 at 1:20,000 (LI-COR) to enable quantification with the LI-COR Odyssey system (LI-COR Biotechnology, Lincoln, NE, USA). Image studio (LI-COR Biotechnology) was used to calculate the ratio of the fully glycosylated upper band (FG)/core-glycosylated lower band (CG) in a manner that was similar to previous reports²⁶.

Electrophysiology. Transiently transfected Piezo1^{-/-} HEK293T cells were plated on 35 mm dishes for patch clamp analysis. The extracellular solution for cell-attached patches contained high K⁺ to zero the membrane potential; it consisted of 90 mM potassium aspartate, 50 mM KCl, 1 mM MgCl₂ and 10 mM HEPES (pH 7.2) adjusted with 5 M KOH. The pipette solution contained either 140 mM CsCl or 140 mM NaCl with 10 mM HEPES (pH 7.2) adjusted with the respective hydroxide. Ethylene glycol-bis(β -aminoethyl ether)-N,N,N',N'-tetraacetic acid (EGTA) was added to control levels of free pipette (extracellular) Ca²⁺ using the online EGTA calculator—Ca-EGTA Calculator TS v1.3—Maxchelator. Negative pressure was applied to patch pipettes using a High Speed Pressure Clamp-1 (ALA Scientific Instruments, Farmingdale, NY, USA) and recorded in millimetres of mercury (mmHg) using a piezoelectric pressure transducer (WPI, Sarasota, FL, USA). Borosilicate glass pipettes (Sigma-Aldrich) were pulled with a vertical pipette puller (PP-83, Narashige, Tokyo, Japan) to produce electrodes with a resistance of 1.8–2.2 M Ω . Single-channel Piezo1 currents were amplified using an AxoPatch 200B amplifier (Axon Instruments, Union City, CA, USA), and data were sampled at a rate of 10 kHz with 1 kHz filtration and analysed using pCLAMP10 software (Axon Instruments). The Boltzmann distribution function was used to describe the dependence of mesoscopic Piezo1 channel currents and open probability, respectively, on the negative pressure applied to patch pipettes. Boltzmann plots were obtained by fitting open probability $P_o \sim I/I_{max}$ versus negative pressure using $P_o/(1 - P_o) = \exp[\alpha(P - P_{1/2})]$, where P is the negative pressure (suction) in mm Hg, $P_{1/2}$ is the negative pressure at which $P_o = 0.5$, and α (mm Hg)⁻¹ is the slope of the plot of $\ln[P_o/(1 - P_o)]$ versus $(P - P_{1/2})$, reflecting the channels' mechanosensitivity.

Single-channel amplitudes were measured by Gaussian fits (Clampfit; Axon Instruments) on an all-points-histogram of current amplitudes over a 2 s period exhibiting only single-channel openings. Conductance was then calculated by regressing a line on the graph of current amplitude vs. holding potential at five separate voltages.

Immunogold labelling and electron microscopy. Cells were grown to 70–80% confluency on fibronectin-coated coverslips before being fixed with 4% w/v paraformaldehyde (PFA) in 100 mM Sorensen's phosphate buffer (pH 7.2) for 20 min. Piezo1 localisation was detected using electron microscopy (EM) with immunogold labelling using nanogold followed by silver enhancement. The protocol was adapted from Biazik et al.⁷⁶ as follows: Free aldehyde was quenched with 0.1 M glycine for 20 min and the cell membranes were permeabilized with 0.005% w/v saponin (containing 0.1% w/v bovine serum albumin in 1× PBS) for 8 min. The samples were then incubated with mouse monoclonal anti-Piezo1 antibody (1:60 dilution, Cat# NBP2-75617, Novus Biologicals) overnight at 4 °C. The next day, the samples were washed and incubated with a secondary antibody that was conjugated with 1.4 nm nanogold (1:60 dilution, Cat# 2002-0.5 mL, Nanoprobes, Yaphank, NY, USA) for 1 h. The labelled cells were then fixed in 2.5% w/v glutaraldehyde for 10 min and quenched with 0.1 M glycine for 20 min. The nanogold was silver enhanced for 7 min using an HQ silver enhancement kit (Cat# 2012-45 mL, Nanoprobes). The silver was further stabilised by gold toning that involved 15 min incubation in 2% w/v sodium acetate, 10 min incubation in 0.05% w/v gold (III) chloride trihydrate (on ice) and 10 min incubation in 0.3% w/v sodium thiosulfate pentahydrate (on ice). Because of the sensitivity to light of the reagents, the silver enhancement and gold toning steps were performed in a dark room under a red light. Finally, the cells were post-fixed with 1% w/v osmium tetroxide + 1.5% w/v potassium ferricyanide for 1 h, *en bloc* stained with 2% w/v uranyl acetate for 20 min, dehydrated in a gradient of ethanol, embedded in Procure resin, and polymerised at 60 °C for 48 h.

Polymerised resin blocks were sectioned using an ultramicrotome (Ultracut 7, Leica Microsystems, Wetzlar, Germany) to generate 60 nm ultra-thin sections that

were collected on 200 mesh copper grids. Sections were post-stained with 2% w/v uranyl acetate and Reynold's lead citrate for 10 min, each before imaging under a transmission electron microscope at 200 kV (G2 Tecnai, FEI, Hillsboro, OR, USA).

Mouse tissue. Tissue collection protocols were approved by the Garvan Institute and St. Vincent's Hospital Animal Ethics Committee and were in accordance with the guidelines of the Australian code for the care and use of animals for scientific purposes (8th edition, National Health and Medical Research Council, Canberra, ACT, Australia, 2013) and the Guide for the Care and Use of Laboratory Animals (8th edition, National Research Council, USA, 2011). Piezo1-Tdtomato mice (The Jackson Laboratory Stock No: 029214) were housed in light boxes and entrained to a 12:12 light: dark cycle for 1 week before the experiments. Mice aged 10 weeks old were euthanized with carbon dioxide, lung tissue harvested and immediately homogenised in RIPA buffer, as above, for protein extraction.

RBC collection. Human RBCs were prepared from blood obtained by venipuncture from the cubital fossa of normal informed-consenting donors under approval from the University of Sydney Human Ethics Committee (signed, approved consent form; Project No. 2012/2882). The blood was anticoagulated with 15 IU mL⁻¹ porcine-gut heparin (Sigma-Aldrich). The blood was centrifuged in 50 mL Falcon tubes at 3000×g for 5 min at 4 °C to sediment the RBCs, and the plasma and buffy coat were removed by vacuum-pump aspiration. RBCs were lysed prior to blotting in RIPA buffer as documented above.

Immunofluorescence and western blotting of unroofed fibroblasts. The unroofing method for selectively isolating basal membranes of cells was adapted from ref. ³⁹. Briefly, human BJ-5ta-hTERT foreskin fibroblasts were seeded onto glass coverslips pre-coated with 90 nM fibronectin (20 μ g mL⁻¹; Cat F1141-5MG, Sigma-Aldrich). After 24 h, the cells were washed with PBS then incubated in an hypo-osmotic buffer containing 2.5 mM triethanolamine (TEA) (pH 7.0) for 3 min at room temperature. The cells were seen to be slightly swollen at this stage in the preparation. Immediately after, the TEA medium was removed and the coverslips were washed with PBS containing protease inhibitor (1 tablet of cOmplete Mini, EDTA-free per 10 mL of 1× PBS) using a fine-tip transfer pipette.

Once the cells were unroofed (the extent of this was assessed under a light microscope: unroofed cells had no nucleus), the coverslips were transferred to 4% v/v PFA in cytoskeleton buffer [CB; 10 mM 2-(N-morpholino) ethanesulfonic acid (MES) pH 6.1, 138 mM KCl, 3 mM MgCl₂, 2 mM EGTA] and left to fix for 10 min. The fixed cells were then labelled for actin, the focal adhesion proteins, and nuclei using, respectively, phalloidin conjugated to AlexaFluor568 (A12380, ThermoScientific), a mouse anti-vinculin antibody (1:200; V9131, Sigma-Aldrich), and DAPI. Images were acquired using a widefield fluorescence microscope at 63× (Ti2-E, Nikon, Tokyo, Japan). Alternatively, after unroofing the cells they were lysed in fresh RIPA buffer prior to western blotting.

Biotinylation. Human BJ-5ta-hTERT foreskin fibroblasts cells were grown to 70–90% confluency on a 60 mm dish before being biotinylated. Cells were washed three times using ice cold PBS and then incubated with biotin buffer (154 mM NaCl, 10 mM HEPES, 3 mM KCl, 1 mM MgCl₂, 0.1 mM CaCl₂, 10 mM glucose, pH 7.6) containing 1 mg/mL Sulfo-NHS-Biotin (ThermoFisher Scientific, EZ-Link™, Lot. No. T1266926) for 1 h on ice. The biotin buffer was then washed off and quenched using 5 mL DMEM containing 25 mM HEPES and 0.25% w/v gelatin for 10 min on ice. Cells were then washed three times using ice cold PBS and solubilized using 1 mL RIPA buffer. Cell lysates were cleared by centrifugation at 13,000×g at 4 °C for 20 min. Hundred microlitre supernatant was taken and supplemented with 2% w/v SDS and 0.8 M urea and designated as the 'input' sample. The remaining supernatant was incubated overnight at 4 °C with 100 μ L Streptavidin-Agarose beads (Sigma-Aldrich, Lot#: SLBR5741V) blocked using 0.5% w/v bovine serum albumin for 1 h. Beads were collected and washed three times using RIPA buffer in a 0.8 mL centrifuge column (ThermoFisher Scientific, Pierce, Cat. No. 89868) with centrifugation at 500 × g at 4 °C for 1 min. Hundred microliter flow-through lysate were taken from the first centrifuge and supplemented with 2% w/v SDS and 0.8 M urea to be the flow-through comparison. For protein elution, beads were loaded with 100 μ L 0.9% w/v NaCl solution supplemented with 2% SDS and 0.8 M urea, and boiled at 65 °C for 5 min. Then they were centrifuged at 500 × g at 4 °C for 1 min in the column, and the biotinylated eluate was collected. Identical protein amounts input, biotinylated and flow-through samples were loaded for western blotting then probed with mouse monoclonal anti-Piezo1 antibody (Cat. No. NBP2-75617, Novus Biologicals) and mouse anti- α -actinin antibody (Santa Cruz Biotechnology, Dallas, TX, USA).

Ca²⁺ imaging. Piezo1^{-/-} HEK293T cells expressing Piezo1 were seeded into a 96-well plate and incubated with 100 μ L of 2 μ M Fura-2-AM in DMEM for 30 min at 37 °C. Ca²⁺ transients were recorded using a 20× objective mounted on a Nikon Ti2e microscope and illuminated with a CoolLED pE-340 Fura LED light source.

Live cell labelling. For live cell membrane protein labelling, Piezo1^{-/-} HEK293T cells were plated on 96-well clear bottom plate (ThermoFisher) coated

with 0.1 mg/mL of Poly-L-Lysine (Sigma). Cells were transfected with WT or mutant Piezo1 containing an extracellular HA tag at position 897 (125 ng cDNA each) with lipofectamine 3000. Sixty to seventy-two hours after transfection, live labelling was performed by incubating the cells with an anti-HA antibody (Sigma, 1:100) for 20 min at 37 °C. The cells were then washed with DMEM six times before incubation with an AlexaFluor 555 conjugated anti-mouse secondary antibody (1:200) for 15 min at room temperature (22 °C). Cells were washed again five times with DMEM and twice with PBS, then fixed with 4% PFA for 20 min at room temperature. PFA was washed off and replaced with PBS before confocal microscopy.

Reporting summary. Further information on research design is available in the Nature Research Reporting Summary linked to this article.

Data availability

The source data for graphs and charts in the main figures are available as Supplementary Data 1 and any remaining information can be obtained from the corresponding author upon reasonable request.

Received: 6 February 2021; Accepted: 5 August 2021;

Published online: 06 September 2021

References

- Coste, B. et al. Piezo1 and Piezo2 are essential components of distinct mechanically activated cation channels. *Science* **330**, 55–60 (2010).
- Coste, B. et al. Piezo proteins are pore-forming subunits of mechanically activated channels. *Nature* **483**, 176–181 (2012).
- Douguet, D., Patel, A., Xu, A., Vanhoutte, P. M. & Honore, E. Piezo ion channels in cardiovascular mechanobiology. *Trends Pharm. Sci.* **40**, 956–970 (2019).
- Beech, D. J. & Kalli, A. C. Force sensing by piezo channels in cardiovascular health and disease. *Arterioscler. Thromb. Vasc. Biol.* **39**, 2228–2239 (2019).
- Syeda, R. et al. Piezo1 channels are inherently mechanosensitive. *Cell Rep.* **17**, 1739–1746 (2016).
- Cox, C. D. et al. Removal of the mechanoprotective influence of the cytoskeleton reveals PIEZO1 is gated by bilayer tension. *Nat. Commun.* **7**, 10366 (2016).
- Lewis, A. H. & Grandl, J. Mechanical sensitivity of Piezo1 ion channels can be tuned by cellular membrane tension. *eLife* **8**, e12088 (2015).
- Romero, L. O. et al. Dietary fatty acids fine-tune Piezo1 mechanical response. *Nat. Commun.* **10**, 1200 (2019).
- Ridone, P. et al. Disruption of membrane cholesterol organization impairs the activity of PIEZO1 channel clusters. *J. Gen. Physiol.* **152**, e201912515 (2020).
- Tsuchiya, M. et al. Cell surface flip-flop of phosphatidylserine is critical for PIEZO1-mediated myotube formation. *Nat. Commun.* **9**, 2049 (2018).
- Shi, J. et al. Sphingomyelinase disables inactivation in endogenous PIEZO1 channels. *Cell Rep.* **33**, 108225 (2020).
- Cox, C. D. & Gottlieb, P. A. Amphipathic molecules modulate PIEZO1 activity. *Biochem. Soc. Trans.* **47**, 1833–1842 (2019).
- Tannous, A., Pisoni, G. B., Hebert, D. N. & Molinari, M. N-linked sugar-regulated protein folding and quality control in the ER. *Semin. Cell Dev. Biol.* **41**, 79–89 (2015).
- Spiro, R. G. Protein glycosylation: nature, distribution, enzymatic formation, and disease implications of glycopeptide bonds. *Glycobiology* **12**, 43R–56R (2002).
- Aebi, M. N-linked protein glycosylation in the ER. *Biochim. Biophys. Acta* **1833**, 2430–2437 (2013).
- Gluzman, R. et al. N-glycans are direct determinants of CFTR folding and stability in secretory and endocytic membrane traffic. *J. Cell Biol.* **184**, 847–862 (2009).
- Gong, Q., Anderson, C. L., January, C. T. & Zhou, Z. Role of glycosylation in cell surface expression and stability of HERG potassium channels. *Am. J. Physiol. Heart Circ. Physiol.* **283**, H77–H84 (2002).
- Vandenberg, J. I. et al. hERG K(+) channels: structure, function, and clinical significance. *Physiol. Rev.* **92**, 1393–1478 (2012).
- Petresca, K., Atanasiu, R., Akhavan, A. & Shrier, A. N-linked glycosylation sites determine HERG channel surface membrane expression. *J. Physiol.* **515**, 41–48 (1999).
- Chang, X. B. et al. Role of N-linked oligosaccharides in the biosynthetic processing of the cystic fibrosis membrane conductance regulator. *J. Cell Sci.* **121**, 2814–2823 (2008).
- Cai, Y. et al. Altered trafficking and stability of polycystins underlie polycystic kidney disease. *J. Clin. Investig.* **124**, 5129–5144 (2014).
- Anderson, C. L. et al. Large-scale mutational analysis of Kv11.1 reveals molecular insights into type 2 long QT syndrome. *Nat. Commun.* **5**, 5535 (2014).
- Ke, Y. et al. Trafficking defects in PAS domain mutant Kv11.1 channels: roles of reduced domain stability and altered domain-domain interactions. *Biochem. J.* **454**, 69–77 (2013).
- Foo, B., Williamson, B., Young, J. C., Lukacs, G. & Shrier, A. hERG quality control and the long QT syndrome. *J. Physiol.* **594**, 2469–2481 (2016).
- Apaja, P. M. et al. Ubiquitination-dependent quality control of hERG K+ channel with acquired and inherited conformational defect at the plasma membrane. *Mol. Biol. Cell* **24**, 3787–3804 (2013).
- Perry, M. D. et al. Rescue of protein expression defects may not be enough to abolish the pro-arrhythmic phenotype of long QT type 2 mutations. *J. Physiol.* **594**, 4031–4049 (2016).
- Fotiou, E. et al. Novel mutations in PIEZO1 cause an autosomal recessive generalized lymphatic dysplasia with non-immune hydrops fetalis. *Nat. Commun.* **6**, 8085 (2015).
- Lukacs, V. et al. Impaired PIEZO1 function in patients with a novel autosomal recessive congenital lymphatic dysplasia. *Nat. Commun.* **6**, 8329 (2015).
- Faucherre, A. et al. Piezo1 is required for outflow tract and aortic valve development. *J. Mol. Cell. Cardiol.* **143**, 51–62 (2020).
- Saotome, K. et al. Structure of the mechanically activated ion channel Piezo1. *Nature* **554**, 481–486 (2018).
- Guo, Y. R. & MacKinnon, R. Structure-based membrane dome mechanism for Piezo mechanosensitivity. *eLife* **6**, e33660 (2017).
- Zhao, Q. et al. Structure and mechanogating mechanism of the Piezo1 channel. *Nature* **554**, 487–492 (2018).
- Vero Li, J., D Cox, C. & Martinac, B. The anchor domain is critical for Piezo1 channel mechanosensitivity. *Channels* **15**, 438–446 (2021).
- Ilkan, Z. et al. Evidence for shear-mediated Ca(2+) entry through mechanosensitive cation channels in human platelets and a megakaryocytic cell line. *J. Biol. Chem.* **292**, 9204–9217 (2017).
- Ranade, S. S. et al. Piezo1, a mechanically activated ion channel, is required for vascular development in mice. *Proc. Natl Acad. Sci. USA* **111**, 10347–10352 (2014).
- Nebenfuhr, A., Ritzenthaler, C. & Robinson, D. G. Brefeldin A: deciphering an enigmatic inhibitor of secretion. *Plant Physiol.* **130**, 1102–1108 (2002).
- Gordon, S. E., Munari, M. & Zagotta, W. N. Visualizing conformational dynamics of proteins in solution and at the cell membrane. *eLife* **7**, e37248 (2018).
- Taraska, J. W. A primer on resolving the nanoscale structure of the plasma membrane with light and electron microscopy. *J. Gen. Physiol.* **151**, 974–985 (2019).
- Kuo, J. C., Han, X., Yates, J. R. 3rd & Waterman, C. M. Isolation of focal adhesion proteins for biochemical and proteomic analysis. *Methods Mol. Biol.* **757**, 297–323 (2012).
- Yao, M. et al. Force-Dependent Piezo1 Recruitment to Focal Adhesions Regulates Adhesion Maturation and Turnover Specifically in non-Transformed cells. *bioRxiv*, (2020).
- Ellefsen, K. L. et al. Myosin-II mediated traction forces evoke localized Piezo1-dependent Ca(2+) flickers. *Commun. Biol.* **2**, 298 (2019).
- Blom, N., Sicheritz-Ponten, T., Gupta, R., Gammeltoft, S. & Brunak, S. Prediction of post-translational glycosylation and phosphorylation of proteins from the amino acid sequence. *Proteomics* **4**, 1633–1649 (2004).
- Wollscheid, B. et al. Mass-spectrometric identification and relative quantification of N-linked cell surface glycoproteins. *Nat. Biotechnol.* **27**, 378–386 (2009).
- Wang, L. et al. Structure and mechanogating of the mammalian tactile channel PIEZO2. *Nature* **573**, 225–229 (2019).
- Lewis, A. H. & Grandl, J. Inactivation kinetics and mechanical gating of Piezo1 ion channels depend on subdomains within the cap. *Cell Rep.* **30**, 870–880 (2020).
- Struwe, W. B. & Robinson, C. V. Relating glycoprotein structural heterogeneity to function—insights from native mass spectrometry. *Curr. Opin. Struct. Biol.* **58**, 241–248 (2019).
- Lai, A. et al. Analyzing the shear-induced sensitization of mechanosensitive ion channel Piezo-1 in human aortic endothelial cells. *J. Cell Physiol.* **236**, 2976–2987 (2021).
- Li, J. et al. Piezo1 integration of vascular architecture with physiological force. *Nature* **515**, 279–282 (2014).
- Botello-Smith, W. M. et al. A mechanism for the activation of the mechanosensitive Piezo1 channel by the small molecule Yoda1. *Nat. Commun.* **10**, 4503 (2019).
- Coste, B. et al. Piezo1 ion channel pore properties are dictated by C-terminal region. *Nat. Commun.* **6**, 7223 (2015).
- Bae, C., Suchyna, T. M., Ziegler, L., Sachs, F. & Gottlieb, P. A. Human PIEZO1 ion channel functions as a split protein. *PLoS ONE* **11**, e0151289 (2016).

52. Wang, Y. et al. The role and mechanism of chaperones Calnexin/Calreticulin in which ALLN selectively rescues the trafficking defective of HERG-A561V mutation. *Biosci. Rep.* **38**, BSR20171269 (2018).
53. Wang, X., Koulov, A. V., Kellner, W. A., Riordan, J. R. & Balch, W. E. Chemical and biological folding contribute to temperature-sensitive DeltaF508 CFTR trafficking. *Traffic* **9**, 1878–1893 (2008).
54. Zheng, W., Nikolae, Y. A., Gracheva, E. O. & Bagriantsev, S. N. Piezo2 integrates mechanical and thermal cues in vertebrate mechanoreceptors. *Proc. Natl Acad. Sci.* **2019**, 10213 (2019).
55. Evans, E. L. et al. Yoda1 analogue (Dooku1) which antagonizes Yoda1-evoked activation of Piezo1 and aortic relaxation. *Br. J. Pharmacol.* **175**, 1744–1759 (2018).
56. Okiyonedo, T. et al. Delta F508 CFTR pool in the endoplasmic reticulum is increased by calnexin overexpression. *Mol. Biol. Cell* **15**, 563–574 (2004).
57. Gong, Q., Jones, M. A. & Zhou, Z. Mechanisms of pharmacological rescue of trafficking-defective hERG mutant channels in human long QT syndrome. *J. Biol. Chem.* **281**, 4069–4074 (2006).
58. Oliveras, A. et al. The unconventional biogenesis of Kv7.1-KCNE1 complexes. *Sci. Adv.* **6**, eaay4472 (2020).
59. Ke, Y., Hunter, M. J., Ng, C. A., Perry, M. D. & Vandenberg, J. I. Role of the cytoplasmic N-terminal Cap and Per-Arnt-Sim (PAS) domain in trafficking and stabilization of Kv11.1 channels. *J. Biol. Chem.* **289**, 13782–13791 (2014).
60. Kanner, S. A., Shuja, Z., Choudhury, P., Jain, A. & Colecraft, H. M. Targeted deubiquitination rescues distinct trafficking-deficient ion channelopathies. *Nat. Methods* **17**, 1245–1253 (2020).
61. Kagan, A., Yu, Z., Fishman, G. I. & McDonald, T. V. The dominant negative LQT2 mutation A561V reduces wild-type HERG expression. *J. Biol. Chem.* **275**, 11241–11248 (2000).
62. Foo, B. et al. Mutation-specific peripheral and ER quality control of hERG channel cell-surface expression. *Sci. Rep.* **9**, 6066 (2019).
63. Smith, J. L. et al. Pharmacological correction of long QT-linked mutations in KCNH2 (hERG) increases the trafficking of Kv11.1 channels stored in the transitional endoplasmic reticulum. *Am. J. Physiol. Cell Physiol.* **305**, C919–930 (2013).
64. Smith, J. L. et al. Trafficking-deficient hERG K(+) channels linked to long QT syndrome are regulated by a microtubule-dependent quality control compartment in the ER. *Am. J. Physiol. Cell Physiol.* **301**, C75–C85 (2011).
65. Zhou, Z., Gong, Q. & January, C. T. Correction of defective protein trafficking of a mutant HERG potassium channel in human long QT syndrome. Pharmacological and temperature effects. *J. Biol. Chem.* **274**, 31123–31126 (1999).
66. Loo, M. A. et al. Perturbation of Hsp90 interaction with nascent CFTR prevents its maturation and accelerates its degradation by the proteasome. *EMBO J.* **17**, 6879–6887 (1998).
67. Owsianik, G., Cao, L. & Nilius, B. Rescue of functional DeltaF508-CFTR channels by co-expression with truncated CFTR constructs in COS-1 cells. *FEBS Lett.* **554**, 173–178 (2003).
68. Bavi, N., Richardson, J., Heu, C., Martinac, B. & Poole, K. PIEZO1-mediated currents are modulated by substrate mechanics. *ACS Nano* **13**, 13545–13559 (2019).
69. Poole, K., Herget, R., Lapatsina, L., Ngo, H. D. & Lewin, G. R. Tuning Piezo ion channels to detect molecular-scale movements relevant for fine touch. *Nat. Commun.* **5**, 3520 (2014).
70. Knoepp, F. et al. Shear force sensing of epithelial Na(+) channel (ENaC) relies on N-glycosylated asparagines in the palm and knuckle domains of alphaENaC. *Proc. Natl Acad. Sci. USA* **117**, 717–726 (2020).
71. Chuntharpursat-Bon, E. et al. Cell adhesion molecule interaction with Piezo1 channels is a mechanism for sub cellular regulation of mechanical sensitivity. *bioRxiv* <https://doi.org/10.1101/602532> (2019).
72. Wang, J., Jiang, J., Yang, X., Wang, L. & Xiao, B. Tethering Piezo channels to the actin cytoskeleton for mechanogating via the E-cadherin- β -catenin mechanotransduction complex. *bioRxiv* <https://doi.org/10.1101/2020.05.12.092148> (2020).
73. Buyan, A. et al. Piezo1 forms specific, functionally important interactions with phosphoinositides and cholesterol. *Biophys. J.* **119**, 1683–1697 (2020).
74. Cox, C. D., Bavi, N. & Martinac, B. Biophysical principles of ion-channel-mediated mechanosensory transduction. *Cell Rep.* **29**, 1–12 (2019).
75. Bae, C., Gnanasambandam, R., Nicolai, C., Sachs, F. & Gottlieb, P. A. Xerocytosis is caused by mutations that alter the kinetics of the mechanosensitive channel PIEZO1. *Proc. Natl Acad. Sci. USA* **110**, E1162–E1168 (2013).
76. Biazik, J., Yla-Anttila, P., Vihinen, H., Jokitalo, E. & Eskelinen, E. L. Ultrastructural relationship of the phagophore with surrounding organelles. *Autophagy* **11**, 439–451 (2015).

Acknowledgements

C.D.C. is supported by an NSW Health EMCR Fellowship. C.D.C. and P.W.K. were supported by Australian Research Council Discovery Project Grant DP190100500. The experiments were in part supported by the Victor Chang Cardiac Research Institute Innovation Centre, funded by the NSW Government.

Author contributions

J.L. carried out patch clamping and western blotting and analysed data. C.N. contributed to western blotting. D.C. did electron microscopy. Z.Z. did live cell labelling. P.W.K. collected and processed red blood cells and wrote the manuscript. Y.Z. and Y.G. carried out animal husbandry and provided mouse tissue. L.J., C.N. and Y.R. conceptualized ideas and designed experiments. M.Y. carried out TIRF microscopy. C.D.C. designed and coordinated the full project. The manuscript was written by C.D.C., J.L., C.N., P.W.K., D.F. and M.F., with contributions from all authors. All authors discussed the results and commented on the paper.

Competing interests

The authors declare no competing interests.

Additional information

Supplementary information The online version contains supplementary material available at <https://doi.org/10.1038/s42003-021-02528-w>.

Correspondence and requests for materials should be addressed to C.D.C.

Reprints and permission information is available at <http://www.nature.com/reprints>

Publisher's note Springer Nature remains neutral with regard to jurisdictional claims in published maps and institutional affiliations.



Open Access This article is licensed under a Creative Commons Attribution 4.0 International License, which permits use, sharing, adaptation, distribution and reproduction in any medium or format, as long as you give appropriate credit to the original author(s) and the source, provide a link to the Creative Commons license, and indicate if changes were made. The images or other third party material in this article are included in the article's Creative Commons license, unless indicated otherwise in a credit line to the material. If material is not included in the article's Creative Commons license and your intended use is not permitted by statutory regulation or exceeds the permitted use, you will need to obtain permission directly from the copyright holder. To view a copy of this license, visit <http://creativecommons.org/licenses/by/4.0/>.

© The Author(s) 2021